

*An edited version of this paper was published by AGU.*

*To view the published open abstract, go to <http://dx.doi.org> and enter the DOI below.*

Schuster, G. L., O. Dubovik, B. N. Holben, and E. E. Clothiaux (2005), Inferring black carbon content and specific absorption from Aerosol Robotic Network (AERONET) aerosol retrievals, *J. Geophys. Res.*, 110, D10S17, doi:10.1029/2004JD004548.

## Inferring Black Carbon Content and Specific Absorption from AERONET Aerosol Retrievals

Gregory L. Schuster

NASA Langley Research Center  
Hampton, Virginia, USA

Oleg Dubovik

Laboratory for Terrestrial Physics  
NASA Goddard Spaceflight Center  
Greenbelt, Maryland, USA  
and  
Goddard Earth Science and Technology Center  
University of Maryland Baltimore County  
Baltimore, Maryland USA

Brent N. Holben

Laboratory for Terrestrial Physics  
NASA Goddard Spaceflight Center  
Greenbelt, Maryland, USA

Eugene E. Clothiaux

The Pennsylvania State University  
University Park, Pennsylvania, USA

### Abstract.

Black carbon is ubiquitous in the atmosphere and the main anthropogenic absorbing particulate. Absorption by black carbon is thought to be comparable to the cooling associated with sulfate aerosols, although present day satellites are incapable of obtaining this measurement and model estimates are highly uncertain. More measurements of black carbon concentration are necessary for improving and validating transport and general circulation models. The aerosol robotics network (AERONET) of 180 worldwide radiometers offers an opportunity to obtain these measurements. We use the Maxwell Garnett effective medium approximation to infer the column-averaged black carbon concentration and specific absorption of Aerosol Robotic Network (AERONET) retrievals at 46 locations. The yearly-averaged black carbon column concentrations exhibit the expected regional dependence, with remote island locations having values about an order of magnitude lower than the continental biomass burning locations. The yearly-averaged black carbon specific absorption cross section is consistent with other measured values,  $9.9 \text{ m}^2 \text{ g}^{-1}$  for 19591 retrievals, but varies from  $7.7$  to  $12.5 \text{ m}^2 \text{ g}^{-1}$ . We attribute this variability to the details of the size distributions and the fraction of black carbon contained in the aerosol mixture. We also used the Maxwell Garnett equations to parameterize the imaginary refractive index with respect to the black carbon volume fraction, enabling simple but accurate absorption estimates for aerosol mixtures when the black carbon fraction and size distribution is known. The black carbon concentrations that we derive from AERONET measurements correctly describe the radiance field and represent an alternative to absorption optical thickness in the link between models and AERONET measurements.

### Index terms

Atmospheric composition and structure

0305 Aerosols and particles  
0345 Pollution – urban and regional  
0394 Instruments and techniques  
Global change  
1640 Remote sensing  
1694 Instruments and techniques

**Key words**

soot, elemental carbon, particulate carbon, absorption cross section, absorption efficiency, emissions inventory

## 1. Introduction

It is often reported that aerosols have slowed global warming by scattering incident solar radiation back into space, and that the impact of anthropogenic aerosols is a global cooling comparable in magnitude (but opposite in sign) to the warming associated with anthropogenic infrared-active gases (Charlson et al., 1991; Charlson et al., 1992; Penner et al., 1992; Harshvardhan, 1993; Schwartz, 1996; Delene and Ogren, 2002). While scattering is the predominant radiative effect of aerosols at shortwave wavelengths (i.e., less than 4  $\mu\text{m}$ ), significant absorption by aerosols occurs at these wavelengths as well (Liou et al., 1996; Haywood et al., 1997; Schult et al., 1997; Myhre et al., 1998; Penner et al., 1998; Jacobson, 2001). The most recent report from the Intergovernmental Panel on Climate Change (IPCC, 2001) estimates that absorption by black carbon aerosols can reduce the direct radiative impact of sulfate aerosols by 50–100 percent. Aerosol absorption is significant enough that the radiative impact of aerosols at the top of the atmosphere could change in sign from cooling to warming in regions of highly absorbing aerosols (Chylek and Coakley, 1974; Charlack and Sellers, 1980; Haywood and Shine, 1995). This is especially important when aerosols are located over highly reflective surfaces such as snow or clouds (Haywood and Shine, 1997). Absorbing aerosols may also be responsible for a second indirect effect, whereby clouds evaporate more rapidly because of absorbing haze and cloud condensation nuclei (Ackerman et al., 2000). A recent study also indicates that such aerosols reduce the albedo of ice and snow and increase melt rates (Hansen and Nazarenko, 2004).

Absorption by nondust aerosols in the atmosphere at wavelengths less than 4  $\mu\text{m}$  is mainly caused by the graphitic form of carbon (Rosen et al., 1978; 1982). This highly absorbing particulate is often called carbon black, soot, elemental carbon, or black carbon in the atmospheric literature. Differences between these species do exist, however. Carbon blacks refers to commercially available spherical particles created in a controlled environment. These particles are composed of concentric graphite platelets with diminishing graphitic order near the center (Hess and Herd, 1993). Their commercial availability simplifies the characterization of their physical and optical properties and these properties are often extrapolated to characterize particulate carbon found in atmospheric soot. Atmospheric soot is produced by the same mechanism as carbon blacks (incomplete combustion), but it also contains a variety of impurities (Novakov, 1982; Bansal and Donnet, 1993). For instance, diesel exhaust soot has a much lower carbon content than commercial carbon blacks ( $\sim 45$  percent versus  $\sim 95$  percent) even though they both exhibit very similar primary particle sizes and graphitic internal structure (Clague et al., 1999). The term elemental carbon implies a purity of substance and is generally reserved for thermal analysis of light absorbing carbon, the philosophy being that the various impurities volatilize at a lower temperature than the graphitic component. The term black carbon is often reserved for optical measurements of light absorbing carbon (A.D.A. Hansen, 2003; www.mageesci.com), which can show excellent agreement with thermal elemental carbon measurements (Moosmuller et al., 1998). We adopt the term black carbon to refer to nonorganic particulate carbon in the atmosphere with the understanding that the optical and physical properties that we obtain from the literature may be associated with carbon blacks or soot.

Current satellite technology does not include aerosol absorption measurements, so global estimates must be obtained from transport models and general circulation models (GCMs). The models are typically initialized with gridded emission inventories of all known significant aerosol sources and assumed size distributions. The aerosols are then transported across the globe, changing in mass and optical properties as the modeled relative humidity changes. Removal

occurs by wet and dry deposition. The carbon emissions inventories used to initialize the models are highly parameterized and created on the basis of multiple sparse datasets (such as fuel use inventories and emission factors). The resulting inventories are uncertain by at least a factor of 2 and this uncertainty is carried forward to the model output (Bond et al., 1998; Cooke et al., 1999; Streets et al., 2001).

Complicating matters further, aerosol models often assume external mixtures so that the hygroscopic growth and radiative impact of each component may be considered separately (Kinne et al., 2003), although internal mixtures of black carbon has been explored in at least one model (Jacobson, 1997). (The external mixture assumption presumes that each aerosol particle contains a single species, whereas multiple species are contained within each particle in an internal aerosol mixture.) Measurements show that black carbon and sulfate concentrations are highly correlated, indicating that these two species may be internally mixed (Pinnick et al., 1993; Krivacsy et al., 2001). This hypothesis is confirmed with high-resolution scanning electron microscopy images (Ebert et al., 2002) and is consistent with the deposition rates required by models to remove carbon from the atmosphere; dry deposition is too slow, so modelers regularly assume a hydrophobic to hydrophilic conversion for wet removal of carbon (Collins et al., 2001). Such a conversion would be unlikely in reality unless the carbon was already mixed with a hydrophilic substance. Sulfate is extremely hydrophilic and created in the same combustion processes as soot, providing a plausible physical substrate for this parameterization.

The external or internal mixing state of black carbon is important because it has a direct impact on the specific absorption (absorption per unit mass of black carbon aerosol particles). Internally mixed carbon has a higher specific absorption because of the increased absorption cross section associated with the larger sizes of the mixed aerosols. Values as high as  $20 \text{ m}^2 \text{ g}^{-1}$  have been observed in the atmosphere and are not possible with external aerosol mixtures, which produce values of only a few  $\text{m}^2 \text{ g}^{-1}$  (Fuller et al., 1999). Regions with some internally mixed aerosols and some externally mixed aerosols will have intermediate values of specific absorption. Specific absorption is also sensitive to the fraction of black carbon within an internal mixture, although this has received less attention (Petzold et al., 1997; Neusub et al., 2002a).

Ultimately, the community desires models that accurately calculate atmospheric absorption, and black carbon specific absorption offers a possible parameterization for relating black carbon concentration to its predominant radiative effect. That is, one could use the specific absorption associated with real aerosol mixtures to convert modeled carbon concentrations to a map of aerosol absorption cross sections (Bond et al., 1998). Unfortunately, the black carbon specific absorption is dependent upon the details of the aerosol size distribution and measurements vary by a factor of 4, making the conversion from black carbon concentration to atmospheric absorption nebulous (Liou et al., 1993).

The reality of this difficulty is demonstrated with two recent studies. Sato et al. (2003) used current aerosol emissions inventories and transport models to calculate absorption optical depths and compared their results to aerosol robotics network (AERONET) measurements at 322 locations worldwide. They found that increasing the black carbon emissions inventories by a factor of 2–4 provided the best match to the AERONET measurements. Park et al. (2003) did a similar study (but geographically limited to the United States) where they compared elemental carbon

concentrations to measurements of the Interagency Monitoring of Protected Visual Environments (IMPROVE) network. The Park et al. (2003) study required a 15 percent increase in the black carbon emissions inventories. Both studies used current emissions inventories and external aerosol mixtures. The differences in these studies suggests that errors in the modeled size distributions are increased by the optics module of the models.

Worldwide black carbon concentration measurements are needed to assess the efficacy of the carbon emissions inventory and transport model output. This requires long-term measurements in many regions, as model success in one region or season does not apply to all regions and seasons (Cooke et al., 1999). AERONET is an automated network of more than 180 surface radiometers located throughout the world (Holben et al., 1998; 2001). The sky radiance measurements obtained by AERONET are inverted to provide column-averaged aerosol refractive indices and size distributions for the AERONET database (Dubovik and King, 2000). The AERONET database provides enough information to derive column-averaged black carbon contents and specific absorptions that correctly describe the radiance field, providing a link between AERONET and the transport models.

In this study, we infer the column averaged black carbon content and specific absorption at 46 AERONET locations, assuming that black carbon is internally mixed with the remaining aerosols. We begin by describing the AERONET aerosol retrieval products in the next section. This is followed by forward calculations of the specific absorption for nine climatological aerosol size distributions (Section 3), which illustrate that specific absorption is sensitive to the volume fraction of black carbon in the aerosol mixture. We describe our inverse calculation next, whereby black carbon concentration and specific absorption are inferred from the AERONET retrieval products at 46 locations in the years 2000 and 2001 (Section 4). A number of assumptions are required for our black carbon retrieval, and these are highlighted with sensitivity studies and a literature review in Sections 5 and 6; although the sensitivity studies indicate an estimated retrieval error of +15 to - 40 percent, we caution that we have not performed a rigorous validation with collocated instrumentation. We develop an empirical relationship between the volume fraction of black carbon in an aerosol mixture and the imaginary refractive index, enabling a simple parameterization of the Maxwell Garnett equations for increased computational speed. Finally, we conclude that “optically equivalent” black carbon concentrations and specific absorptions can be inferred from the worldwide AERONET data products.

## 2. The AERONET product

AERONET is described in detail in Holben et al. (1998). It consists of more than 180 sun and sky scanning radiometers located at surface sites throughout the world. The radiometers have a narrow field of view (1.2 degrees) and are mounted on programmable trackers, enabling direct sun measurements as well as sky radiance measurements. A filter wheel allows measurements in up to 8 spectral bands, typically centered at 0.34, 0.38, 0.44, 0.50, 0.67, 0.87, 0.94, and 1.02  $\mu\text{m}$ . Each band has a full width of approximately 0.010  $\mu\text{m}$  at half maximum (FWHM). All of these spectral bands are utilized in the direct sun measurements, but only four of them are used for the sky radiance measurements (0.44, 0.67, 0.87, and 1.02  $\mu\text{m}$ ). Instruments are calibrated on a 6-month rotation and the optical filters are changed every 2 years.

### 2.1. Almicantar Radiance Scan Retrievals

One component of the sky radiance measurements is the almicantar scan, which forms the basis of the size distribution

and refractive index retrievals in the AERONET database (Dubovik and King, 2000). This scan provides radiances at the solar zenith angle and 76 relative azimuth angles, nearly covering the full azimuthal circle. An azimuthal symmetry requirement eliminates some measurements but at least 21 angles must survive for a quality retrieval. A homogeneous mixture of molecules and aerosols is assumed for the retrieval and the aerosol properties are adjusted until a forward radiation model matches the measurements in a “best fit” sense. The retrieval provides the aerosol volume size distribution ( $dV/d\ln r$ ) for 22 radii between 0.05 and 15  $\mu\text{m}$  (integrated over the atmospheric column) and the refractive index at the scanning wavelengths. The size distribution accuracy expected for fine-mode dominated aerosols is 15-25 percent for radii between 0.1 and 7  $\mu\text{m}$ , 25-100 percent otherwise. The real refractive index is expected to be accurate to 0.04, the imaginary refractive index accurate to 30-50 percent for aerosol optical thicknesses greater than 0.4 at the 0.440  $\mu\text{m}$  wavelength. The uncertainties are higher for coarse-mode dominated aerosols such as dust and optically-thin aerosols. An accuracy assessment of the AERONET retrievals can be found in Dubovik et al. (2000).

We emphasize that the AERONET size distributions and refractive indices are obtained from a radiative retrieval, and as such they correctly describe the radiance field. Throughout this paper we consider only AERONET retrievals with averaged residual radiance errors less than 5 percent obtained over at least 21 azimuth angles. Solar zenith angles must be greater than 45 degrees but less than 77 degrees. The minimum solar zenith angle of 45 degrees assures a retrieval based upon scattering angles of at least 90 degrees (the maximum scattering angle in an almicantar measurement occurs at twice the solar zenith angle). The maximum scattering angle of 77 degrees assures validity of the plane parallel assumption for radiative transfer calculations (which is violated by curvature effects when the sun is near the horizon). We include no restriction on aerosol optical depth, as our testing indicates that accurate surface irradiances are obtained with these restrictions on the AERONET retrievals, even at low optical depths (G. Schuster Ph.D. Thesis; www.etd.psu.edu).

### 2.2. Climatologies

The AERONET database has been operational at some sites since 1993, resulting in a new climatological dataset that is summarized in Dubovik et al. (2002). Briefly, this climatology provides averaged aerosol size distributions, refractive indices, and optical depths at 12 regions worldwide. The size distributions are presented as bimodal lognormal distributions in their Equation (1):

$$\frac{dV(r)}{d\ln r} = \sum_{i=1}^2 \frac{C_{v,i}}{\sqrt{2\pi}\sigma_i} \exp\left[-\frac{(\ln r - \ln r_{v,i})^2}{2\sigma_i^2}\right]. \quad (1)$$

Here,  $C_{v,i}$  represents the particle volume concentration,  $r_{v,i}$  is the median radius, and  $\sigma_i$  is the standard deviation of each mode. These parameters and other aerosol optical properties are summarized for the 12 regions in their Table 1. Their parameterizations include four urban-industrial climatologies (GSFC at the Goddard Space Flight Center in Greenbelt, Maryland; Crete-Paris in Europe; Mexico City; and Maldives/INDOEX near India), four biomass burning climatologies (Amazonian Forest, Brazil; South American cerrado, Brazil; African savanna, Zambia; Boreal Forest, U.S.A. and Canada), three desert dust climatologies (Bahrain-Persian Gulf; Solar Village, Saudi Arabia; Cape Verde) and one oceanic climatology (Lanai, Hawaii). In Section 3.2, we use nine of the twelve AERONET climatologies (all nondust) to demonstrate that the specific absorption of internally mixed black carbon is sensitive to the details of the aerosol size distribution and the volume fraction of black carbon.

### 3. Effect of Aerosol Morphology on Black Carbon Specific Absorption

Surface measurements of black carbon specific absorption indicate a large range of values, and this is often attributed to the degree of internal or external mixing of an aerosol size distribution (Liou et al., 1993). Indeed, Ackerman and Toon (1981) found black carbon spheres coated with uniform sulfate shells to be more absorbing than external mixtures with equivalent volume mixing ratios. This is caused by two effects: 1.) the sulfate coating increases the effective absorption cross sectional area of the carbon particles (radiation that would otherwise miss the black carbon particle is refracted into it by the sulfate coating) and 2.) varying the volume mixing ratio of black carbon while maintaining the same total size distribution necessarily varies the size of the soot particles in the concentric sphere model. The specific absorption decreases with respect to particle size because black carbon is extremely absorbing, with an e-folding distance of the order of  $0.05 \mu\text{m}$  at a wavelength of  $0.55 \mu\text{m}$ . Hence, molecules at the center of soot particles with radii much larger than  $0.05 \mu\text{m}$  contribute to the mass but not the absorption because they are shielded from incident radiation by the perimeter molecules.

We discuss some possible internal mixture scenarios in Section 3.1 and methods for calculating the associated aerosol optical properties. Then we use nine AERONET climatological size distributions to show that the measured specific absorption variability can be explained with aerosols that are exclusively internally mixed (Section 3.2).

#### 3.1. Effective Medium Approximations for Internal Aerosol Mixtures

Chain aggregates of soot containing soluble compounds can collapse to form sphere-like structures when subjected to increasing relative humidity (Hallet et al., 1989) and are often encapsulated in sulfate (Ebert et al., 2002). This type of aerosol lends itself to a concentric sphere model of a carbon core within a sulfate shell. Alternatively, very small carbon particles may be spread throughout a sulfate host aerosol. (Here, small means that the electric field is uniform throughout the particle.) We can calculate an effective refractive index for such a mixture and use Mie theory to determine the optical properties. There are a variety of effective medium approximations available for this purpose; the Maxwell Garnett effective medium approximation is appropriate for homogeneous mixtures of small insoluble particles suspended in a solution (Lesins et al., 2002). The Maxwell Garnett and concentric sphere models will render different optical properties for equivalent volume fractions of black carbon, and neither of them can be expected to accurately describe all aerosol mixtures in the atmosphere.

An ensemble average of black carbon inclusions at all positions within a nonabsorbing host aerosol is probably a more realistic way to compute aerosol optical properties (i.e., a position-averaged model). Unfortunately, calculations of this type are computationally expensive and unamenable to routine processing of a variety of size distributions (Chylek et al., 1995; Fuller et al., 1999). However, the position-averaged model is useful for assessing the accuracy of the Maxwell Garnett and concentric sphere models in select cases, as was done by Fuller et al. (1999). They compared the specific absorption ( $\lambda = 0.55 \mu\text{m}$ ) calculated with all three models for mass fractions of carbon from 0.01 to 0.2 and composite particle radii up to  $1 \mu\text{m}$ . (Atmospheric aerosols typically have mass fractions of elemental carbon less than 0.2; Malm et al., 1994.) Fuller et al. (1999) found that the position-averaged specific absorption equals or exceeds the Maxwell Garnett values for host radii less than

about  $0.2 \mu\text{m}$  but is less than the concentric sphere specific absorption in this size range. At larger radii, the position-averaged and concentric sphere specific absorption converges to a value below the Maxwell Garnett values. Hence, we can use the concentric sphere and Maxwell Garnett models to estimate the range of specific absorption for internally mixed atmospheric aerosols.

#### 3.2. Specific Absorption of the AERONET Climatologies

We used the concentric sphere, Maxwell Garnett, and an external mixture model to calculate the range of specific absorption (at  $\lambda = 0.55 \mu\text{m}$ ) of the nine AERONET non-dust climatological size distributions in Dubovik et al., 2002 (GSFC, Crete-Paris, Mexico City, Maldives-INDOEX, Amazon Forest, South American Cerrado, African Savannah, Boreal Forest, and Lanai). We used the average optical depths listed in their Table 1 for the volume concentrations, median radii, and standard deviations necessary to describe the bimodal lognormal size distributions of their Equation 1. We assumed a mixture of black carbon with ammonium sulfate to approximate a dry aerosol mixture, allowing the volume fraction of black carbon to vary from 0 to 1 (which necessarily adjusted the composite refractive index for the Maxwell Garnett model). We then used standard algorithms to calculate the absorption component of the optical thickness (Wiscombe, 1980; Toon and Ackerman, 1981) and divided by the black carbon concentration to obtain the black carbon specific absorption in units of  $\text{m}^2 \text{g}^{-1}$ . For the external mixture, we assume that all of the black carbon is confined to the fine mode (radii less than  $0.6 \mu\text{m}$ ) in equal volume fractions at each radius and we perform the calculations for a 3-mode distribution (fine mode black carbon, fine and coarse mode sulfate). However, at black carbon fractions greater than the fine mode fraction we allow black carbon in the coarse mode in equal fractions at each coarse mode radius. (That is, we allow the coarse mode to fill after the fine mode has been completely occupied with black carbon). We use a black carbon refractive index of  $2 - 1i$  (Janzen, 1979) and an ammonium sulfate refractive index of  $1.53 - 10^{-7}i$  (Toon et al., 1976).

The range of specific absorption calculated using the concentric sphere and Maxwell Garnett models for all nine non-dust climatologies is indicated by the shaded area in Figure 1; the bar in Figure 1 indicates the range of values calculated with fine mode black carbon in the external mixture model. The lines in Figure 1 correspond to the GSFC climatology with different mixing scenarios and are qualitatively similar to the other climatologies. Scaling the various size distributions to a single optical depth had no effect on the results because the specific absorption is sensitive to the shape of the size distribution and not the magnitude.

As expected, the concentric sphere specific absorption (dashed line) is greater than the Maxwell Garnett specific absorption (solid line) at the low black carbon fractions common for atmospheric aerosols. This is because low black carbon fractions correspond to small cores that are efficient absorbers in the concentric sphere model, and concentric black carbon cores are more efficient absorbers than eccentric black carbon cores (Fuller et al., 1999). Small, efficient absorbers are assumed to be located throughout the host for the Maxwell Garnett effective medium approximation, but some of the absorbers are in eccentric positions (and hence less efficient). At larger volume fractions of black carbon the concentric sphere model uses larger core particle sizes that are less efficient absorbers than their smaller counterparts. No such size increase is incurred for the Maxwell Garnett effective medium approximation, so this model becomes the more efficient absorbing scenario.

The external mixture specific absorption (long dashes) remains constant at  $4.3 \text{ m}^2 \text{g}^{-1}$  when the black carbon is confined to the fine mode because the shape of the black carbon size distribution remains constant. It decreases when

the volume fraction of black carbon for the external mixture exceeds the fine mode volume fraction, indicative of the changing shape of the now bimodal black carbon distribution. All three mixtures (Maxwell Garnett, concentric sphere, and external) converge to the same specific absorption of  $2.8 \text{ m}^2 \text{ g}^{-1}$  when the volume fraction of black carbon approaches unity. (Incidentally, this is the same specific absorption that is obtained for any volume fraction of black carbon when it is externally mixed with equal fractions at all radii in the GSFC climatology.) There is a region where the external mixture is more absorbing than the internal mixture because particle absorption efficiency is greater in the fine mode. Recall that the fine mode is completely occupied before any black carbon is added to the coarse mode in our external mixing scheme, whereas the two modes are occupied at the same fraction in the internal mixing scheme. The internal mixture is always more absorbing than an external mixture with equivalent volume fractions of black carbon at each radii.

The specific absorption for both internal mixtures are a factor of 1.9-2.8 greater than the external mixture for black carbon fractions less than 5 percent. This enhanced absorption is caused by the increased number of absorbers associated with the internal mixtures (i.e., a system with many slightly absorbing particles is more absorbing than a system with a few highly absorbing particles). As the volume fraction of black carbon increases the effect becomes less obvious because the number of absorbers of the external mixture approaches the number of absorbers of the internal mixture. Likewise, the effective refractive index of the internal mixture approaches the refractive index of the external mixture.

Recognizing that the specific absorption is sensitive to the chosen size distributions, we also calculated (but do not show) the specific absorption for external mixtures utilizing black carbon particle size distributions identical to the black carbon core sizes of our concentric sphere models. The specific absorption varies with the volume fraction of black carbon for this type of external mixture, but the maximum specific absorption for the GSFC climatology is still only  $4.5 \text{ m}^2 \text{ g}^{-1}$ , and the maximum for all of the AERONET climatologies is  $4.9 \text{ m}^2 \text{ g}^{-1}$  (occurring at a black carbon volume fraction of about 5 percent). This indicates that the enhanced absorption of the concentric sphere model shown in Figure 1 is not caused by the variable black carbon core sizes in that model.

The results in Figure 1 are consistent with measurements of ambient aerosols at visible wavelengths by other authors. The inverse relationship between specific absorption and the fraction of black carbon aerosol has been observed with *in situ* measurements (Petzold et al., 1997; Neusub et al., 2002a). Moosmuller et al. (1998) observed  $10 \text{ m}^2 \text{ g}^{-1}$  (at a wavelength  $\lambda$  of  $0.532 \mu\text{m}$ ) using photoacoustic and filter-based measurements during the winter in Brighton, Colorado. Arnott et al. (2003) measured  $8.1 \text{ m}^2 \text{ g}^{-1}$  during the summer and fall at the Big Bend National Park in Texas using the same technique. Hartley et al. (2000) found that  $14 \text{ m}^2 \text{ g}^{-1}$  ( $\lambda = 0.535 \mu\text{m}$ ) was the best fit to all of their flight data in the summer over the Atlantic Ocean. Indeed, Liousse et al. (1993) measured specific absorptions from 5 to  $20 \text{ m}^2 \text{ g}^{-1}$  (wavelength unspecified) for ambient aerosols, and speculated that the differences are caused by variability in the aerosol mixing state (internal or external).

Laboratory-generated aerosols seem to produce lower values. Colbeck et al. (1997) measured 3 to  $8.1 \text{ m}^2 \text{ g}^{-1}$  ( $\lambda = 0.632 \mu\text{m}$ ) for various smokes, depending upon the type of fuel chosen for the experiment. Bruce et al. (1991) measured  $4.55 \text{ m}^2 \text{ g}^{-1}$  ( $\lambda = 0.488 \mu\text{m}$ ) for diesel fuel burned on a wick. Since laboratory measurements are obtained for fresh aerosols close to the source, they probably represent external mixtures or internal mixtures with black carbon fractions greater than commonly found in atmospheric aerosols (i.e., regions to the right in Figure 1).

Figure 1 illustrates that the range of black carbon specific absorption measurements found in the literature can be

explained with the details of the size distribution and the volume fraction of black carbon. This result is independent of the combustion process, as we used the same refractive indices in all tests. We used nine plausible size distributions to define the shaded area in Figure 1, which indicates a large variability associated with *internal* aerosol mixtures. We discuss the implications of aerosol morphology on black carbon specific absorption further in the next section when we show similar results for real AERONET retrievals using wet aerosols (i.e., 3-component mixtures).

## 4. Black Carbon Content and Specific Absorption at AERONET sites

In previous sections, we argued that internal mixtures of black carbon predominate external mixtures of black carbon, mainly on the grounds that black carbon specific absorptions of  $10 \text{ m}^2 \text{ g}^{-1}$  can not be achieved with realistic external mixtures (Fuller et al., 1999). An internal mixture is also inherently assumed in the AERONET almucantar retrievals, as particles of all sizes are assumed to have the same refractive index (Dubovik and King, 2000). This enables the use of the Maxwell Garnett effective medium approximation to deduce the black carbon concentration associated with the AERONET refractive index retrievals. Choosing another mixing scenario (such as the concentric sphere model) will require adjustments in other aerosol properties to accurately describe the almucantar radiances, effectively undoing the original retrieval.

In this section, we use the Maxwell Garnett effective medium approximation and a 3-component mixture of water, ammonium sulfate, and black carbon to deduce the black carbon concentration and specific absorption for the AERONET size distribution and refractive index retrievals. We apply the method at five locations where longterm retrievals are available and show a seasonal variability in black carbon concentration. We use the same method at 46 AERONET sites for the years 2000 and 2001, and show that black carbon specific absorption is highly variable but consistent with the surface measurements of other authors. Regional concentrations of black carbon behave as expected, with the lowest values at remote island sites, higher values at continental sites, and the highest values at biomass burning sites.

### 4.1. Applying Maxwell Garnett Equations to Real-time AERONET Retrievals

The complex refractive index at one or more wavelengths may be used to determine the volume fraction of three known components in an internally mixed aerosol distribution. Ideally, the three aerosol components are obtained from compositional analysis, but the deduced volume fraction of black carbon is nearly independent of the other constituents if it is the only absorber at the observed wavelengths. We demonstrate the technique here using a water aerosol with black carbon and ammonium sulfate inclusions, but other components will work as well. These components were chosen because they were frequently found during the tropospheric aerosol radiative forcing experiment (TARFOX, Hegg et al., 1997) and the Lindenberg aerosol characterization experiment (LACE 98; Ebert et al., 2002), indicating that this composition of aerosols is usually present in hazy urban regions.

The Maxwell Garnett effective medium approximation allows the computation of the average dielectric function based upon the average electric fields and polarizations of a

host matrix with embedded inclusions, and is the appropriate effective medium approximation for mixtures of insoluble particles suspended in solution (Bohren and Huffman, 1983; Lesins et al., 2002). Since most aerosol particles are not chemically bound to water (Seinfeld and Pandis, p. 507), the Maxwell Garnett effective medium approximation is appropriate for solutions of soluble ammonium sulfate with water and black carbon as well. The inclusions must be small with respect to the irradiating wavelength because the electric field is assumed to be uniform throughout the inclusions (even though the size of the inclusions is unspecified in the Maxwell Garnett equations). Inevitably, this small particle assumption is sometimes violated with atmospheric black carbon, so we discuss the repercussions of using the Maxwell Garnett equations on real world aerosols in Section 6.3.

The dielectric functions of atmospheric aerosols are not typically tabulated in the literature, so they must be computed from the square of the refractive index. Once the dielectric functions are known for the host and its constituents, the Maxwell Garnett dielectric function may be calculated for a homogeneous material containing two types of spherical inclusions (Bohren and Huffman, 1983):

$$\varepsilon_{MG} = \varepsilon_m \left[ 1 + \frac{3(f_1 \frac{\varepsilon_1 - \varepsilon_m}{\varepsilon_1 + 2\varepsilon_m} + f_2 \frac{\varepsilon_2 - \varepsilon_m}{\varepsilon_2 + 2\varepsilon_m})}{1 - f_1 \frac{\varepsilon_1 - \varepsilon_m}{\varepsilon_1 + 2\varepsilon_m} - f_2 \frac{\varepsilon_2 - \varepsilon_m}{\varepsilon_2 + 2\varepsilon_m}} \right], \quad (2)$$

where  $\varepsilon_m$ ,  $\varepsilon_1$ , and  $\varepsilon_2$  are the complex dielectric functions of the host matrix and inclusions, and  $f_1$ ,  $f_2$  are the volume fractions of the inclusions. (Note that we used the special case of  $f_2 = 0$  for the calculations of the 2-component mixture in Section 3.) Then the following relations are used to obtain the corresponding refractive index of the mixture:

$$m_r = \sqrt{\frac{\sqrt{\varepsilon_r^2 + \varepsilon_i^2} + \varepsilon_r}{2}}, \quad (3)$$

and

$$m_i = \sqrt{\frac{\sqrt{\varepsilon_r^2 + \varepsilon_i^2} - \varepsilon_r}{2}}, \quad (4)$$

where  $\varepsilon_r$  and  $\varepsilon_i$  represent the real and imaginary components of the mixture dielectric function,  $\varepsilon_{MG}$ .

This establishes a procedure for calculating the effective complex refractive index of an aerosol given a host material and the volume fractions of two inclusions. However, we are interested in the inverse process; we would like to calculate the volume fraction of the inclusions from the aerosol complex refractive index in the AERONET database. To achieve this result, we adjust the volume fraction of the inclusions until the  $\chi^2$ -fit of the complex refractive index for the mixture to the retrieved values in the AERONET database is minimized:

$$\chi^2 = \sum_{l=1}^4 \frac{(m_l^{trv} - m_l^{mix})^2}{m_l^{trv}}, \quad (5)$$

where  $m_l^{trv}$  are the retrieved refractive indices,  $m_l^{mix}$  are the calculated refractive indices for the mixture, and  $l$  is the summation index over the four retrieval wavelengths. The extremely small imaginary refractive index of most noncarbon aerosols in the visible range ( $\sim 10^{-7}$ ) allows the  $\chi^2$ -fit for the imaginary and real components to be computed separately. First, the volume fraction of black carbon in a black carbon and water mixture is adjusted until a minimum  $\chi^2$ -fit to the imaginary refractive index is obtained. Then the volume fraction of black carbon is held constant, and the volume fraction of ammonium sulfate in a mixture of ammonium sulfate, black carbon, and water is adjusted until a minimum  $\chi^2$ -fit to the real refractive index is obtained.

Since the imaginary refractive index of ammonium sulfate is extremely small, it does not perturb the imaginary refractive index of the mixture and no further adjustment is necessary.

The black carbon fraction ( $f_{bc}$ ) thus obtained can be converted to column-integrated black carbon concentration through multiplication by the black carbon density ( $\rho_{bc}$ ) and the size-integrated aerosol volume distribution:

$$[BC] = f_{bc} \rho_{bc} \int \frac{dV}{dlnr} dlnr, \quad (6)$$

where  $V$  is particle volume and  $r$  is particle radius. The units in Equation (6) are mass per unit area because  $V$  represents a column-integrated concentration with units of volume per unit area. The black carbon concentration obtained in this manner can be used in conjunction with the absorption optical depth to obtain the specific absorption cross section in units of  $\text{m}^2 \text{g}^{-1}$ :

$$\alpha = \frac{\tau_a}{[BC]}. \quad (7)$$

The black carbon concentrations and specific absorptions computed in this manner are thus constrained by the refractive indices and size distributions in the AERONET database. Alternatively, one could choose a single value for  $\alpha$  (such as  $10 \text{ m}^2 \text{g}^{-1}$ ) and deduce a black carbon concentration from  $\tau_a$  and Equation (7), but this does not properly account for the variable specific absorption associated with the particle size distribution and black carbon fraction.

#### 4.2. Inferred Concentration of Black Carbon at Selected AERONET Locations for 1993-2002

The column-averaged black carbon concentration was calculated using Equation (6) and the almucantar retrievals at five AERONET sites for all available instantaneous data in the period from 1993 through 2002; the results are shown in Figure 2. The Mongu and Alta Floresta sites are at biomass burning locations in Africa and South America; the Goddard Space Flight Center (GSFC) site is at an urban location (Washington DC metropolitan area) subject mainly to automobile exhaust; the Clouds and Radiation Testbed site (CART) is in central Oklahoma (USA) at a rural location; the Mauna Loa site is located on a mountaintop in Hawaii and is often representative of background aerosols.

The deduced black carbon at these locations behaves as expected. The Mauna Loa site is characterized by background levels of black carbon throughout the year (less than  $0.5 \text{ mg m}^{-2}$ ) with slightly higher values in the spring and summer months. It is probable that these slight perturbations are caused by dust transported from Asia. The rural aerosols at the CART site are also characterized by low black carbon concentrations (less than  $1.0 \text{ mg m}^{-2}$ ) but the frequency and the magnitude of the anomalies is much greater, indicative of a location closer to combustion sources. The urban aerosols at GSFC have much higher black carbon loading throughout the year. Additionally, a seasonal variation is apparent at GSFC during the 6 years of this data set. Black carbon loading is always lower at the beginning and end of the year than it is during the spring and summer months, possibly caused by increased automobile traffic during these time periods. This seasonal variability is not correlated with aerosol optical depth or column-integrated water vapor. Seasonal variation is even more obvious at the biomass burning sites.

#### 4.3. Black Carbon Retrievals at 46 AERONET Locations for 2000-2001

We used the refractive index and size distributions at the 46 AERONET sites listed in Table 1 with Maxwell Garnett  $\chi^2$ -iteration (Eq. 5) to calculate the black carbon fractions and specific absorptions using Equation (7), focusing

on nondust regions where 50 or more retrievals are available in the years 2000 and 2001. Descriptions of many of the sites may be found in Holben et al. (2001). We used aerosol climatology to chose the nondust regions, avoiding locations in Asia, North Africa, and the Middle East that are sometimes prone to dust storms. Nonetheless, we recognize that dust is expected to play a role at many of the sites that we have chosen; we discuss dust contamination of the retrieval in Section 5.1. The range of specific absorptions and black carbon fractions at all of these sites is shown in Figure 3; note that they are similar to the shaded area for the nine climatologies shown in Figure 1.

The GSFC site is highlighted to show the variability exhibited at an individual site. Note the highly variable specific absorption at this site for black carbon fractions less than 0.02 (about 6 to 14  $\text{m}^2 \text{g}^{-1}$ ). Variable black carbon specific absorptions are common to all 46 AERONET sites. This variability is not caused by different combustion processes affecting the optical properties of soot, as we used the same refractive index for black carbon in all cases. Likewise, we consistently assumed that all size distributions are composed of spherical aerosols with internal black carbon inclusions, so aerosol morphology is not the culprit.

The variability is more easily explained with the shaded area of Figure 1. Vertical displacements in this area represent a single aerosol black carbon fraction (and hence, a single imaginary refractive index for the aerosol mixture), but a variety of bimodal lognormal size distributions. Hence, the corresponding changes in specific absorption are caused by the varying absorption efficiencies associated with the size of the particles. For instance, Figure 1 indicates that a homogeneous mixture of 10 percent black carbon with ammonium sulfate in the GSFC climatological size distribution will produce a black carbon specific absorption of  $8.3 \text{ m}^2 \text{g}^{-1}$ . However, the shaded region indicates specific absorptions of 4.2 to  $9.6 \text{ m}^2 \text{g}^{-1}$  are possible for the same fraction of black carbon. Likewise, changing the amount of black carbon in a given size distribution will change the optical properties of the internally mixed aerosol. An example of this effect is shown by the solid line in Figure 1 for the GSFC climatological size distribution, which indicates that the specific absorption varies from 9.75 to  $7.1 \text{ m}^2 \text{g}^{-1}$  for the black carbon fraction 0 to 0.2 commonly found in the atmosphere (Malm et al., 1994). In this case, the size distribution of the mixture remains constant but the soot content of the mixture changes.

The data in figures 1 and 3 indicate that the large variation in specific absorption found in the literature could be caused by different internally mixed size distributions and black carbon fractions. In the example cited above, one might conclude that the size distribution effects dominate because the specific absorption varied by a factor of 2.3 (i.e.,  $9.6/4.2$ ) for the range of aerosol distributions when the black carbon content was held constant at 10 percent, but it only varied by a factor of 1.37 ( $9.75/7.1$ ) for a single aerosol size distribution. This is deceptive, however, as the wide array of size distributions for the nine aerosol climatologies of Figure 1 does not exist at all AERONET sites. We found no simple relationship between the specific absorption and any single mode property of these bimodal distributions (i.e., modal effective radii, standard deviations, and volume concentrations).

Although we observe some extraneous low values near  $5 \text{ m}^2 \text{g}^{-1}$  as reported elsewhere, we never observe the opposite extreme values of  $20 \text{ m}^2 \text{g}^{-1}$ . As stated earlier, however, the Maxwell Garnett mixing rule tends to underestimate the specific absorption with respect to position-averaging of single inclusions for the black carbon fractions typically found in the atmosphere (Fuller et al., 1999). The specific absorption at any given location is highly sporadic on a daily basis, as shown for the year 2000 at the GSFC site in Figure

4, indicating that short-term *in situ* measurements may not necessarily represent climatological values.

The yearly-averaged specific absorption for the 46 AERONET sites is shown in Table 1. The results are also shown in Figure 5 with latitude as the abscissa (to aid in comparisons with the table). The whiskers in Figure 5 represent one standard deviation in the yearly data set, indicating the large variability found at any AERONET site. The island sites tend to have the highest values, ranging from  $8.8 \text{ m}^2 \text{g}^{-1}$  at Tahiti to  $12.6 \text{ m}^2 \text{g}^{-1}$  at the Dry Tortugas. Values at the continental sites (North and Central America, Europe, and Asia) are slightly lower, ranging from  $8.1 \text{ m}^2 \text{g}^{-1}$  at Boulder to  $11.4 \text{ m}^2 \text{g}^{-1}$  at the CART site. The biomass burning sites in South America and South Africa have the lowest specific absorptions:  $7.15 \text{ m}^2 \text{g}^{-1}$  at Cuiaba-Miranda to  $10.6 \text{ m}^2 \text{g}^{-1}$  at Alta Floresta.

These yearly-averaged results are consistent with the instantaneous data of Figure 3, which indicates that the highest specific absorption corresponds to the lowest fractions of black carbon. Hence, the clean island sites have a higher specific absorption than the continental sites, which are typically located closer to sources of black carbon. The biomass burning sites are located near very strong sources of black carbon emissions, resulting in even higher fractions of black carbon and the lowest specific absorption. This effect is enhanced at sites where the data are acquired only during the burning season. These regional averages are summarized in Table 2.

The corresponding column-averaged black carbon concentration at these sites is shown in Figure 6. The greatest black carbon concentrations are found at the biomass burning sites and the lowest concentrations at the remote island sites (consistent with comments in the previous paragraph). Comparison with *in situ* measurements of black carbon concentration is difficult because of different sampling volumes, but *in situ* techniques typically produce values of less than  $13.3 \mu\text{g m}^{-3}$  at urban locations and less than  $0.3 \mu\text{g m}^{-3}$  in remote areas (Allen et al., 1999; Pinnick et al., 1993; Seinfeld and Pandis, 1998). If these concentrations were well-mixed in a 1-km boundary layer the corresponding column-averaged concentrations would be  $13.3 \text{ mg m}^{-2}$  and  $0.3 \text{ mg m}^{-2}$ . All of the continental and biomass burning sites fall within this range of values, as do most of the island sites in Figure 6.

## 5. Sensitivity of Black Carbon Fraction and Specific Absorption to Aerosol Optical Properties

Although the AERONET database provides the refractive index associated with internal aerosol mixtures, it does not provide information about the aerosol components within the mixture. We assumed that the aerosol components were water, ammonium sulfate, and black carbon when we outlined our procedure in Section 4.1. The uncertainty in our retrievals associated with using this three-component mixture for all aerosols is quantified with a sensitivity study in Section 5.1. We found that the results are sensitive to the *real* refractive index of the host but not the 2nd inclusion, a result that we exploit in Section 5.2.

The refractive index of particulate soot is notoriously difficult to measure, so we include another sensitivity study to assess the impact of using various measured values on our retrievals in Section 5.3. We discuss some of the available measurements and our rationale for choosing  $m = 2 - 1i$  for our retrievals. Finally, we discuss the sensitivity of our retrieval to the density of black carbon and possible organic carbon absorption.

We test our retrieval by applying the procedure to other aerosol mixtures. Comparison of the inferred black carbon using other mixtures to the inferred black carbon using our original mixture of water, ammonium sulfate, and black carbon forms the basis of our first sensitivity study.

### 5.1. Choice of Host Aerosol

Black carbon is ubiquitous in the atmosphere and is found in the most remote locations, including background aerosols in the Arctic (Rosen et al., 1982). It is undoubtedly the dominant absorber in the AERONET retrievals when significant dust concentrations are not present. The other two components of our assumed aerosol mixture (water and ammonium sulfate) might not be present, however. We investigated the impact of using various common aerosols — water, sea salt, ammonium sulfate, ammonium nitrate, dust — as hosts and inclusions in our three-component mixture, always including black carbon inclusions. We tested the black carbon retrieval with these various components at the CART, COVE, GSFC, and Lanai sites for the years 2000 and 2001 (2982 retrievals) and compared the deduced black carbon fractions with the baseline case of a water host with ammonium sulfate and black carbon inclusions.

We found that the results are sensitive to the refractive index of the host but not the 2nd inclusion. The real refractive index of both the host aerosol and the black carbon inclusions has a significant effect on our retrieval because the imaginary and real refractive indices of the mixture are interdependent (Equations 2-4). However, the imaginary refractive indices of the nonabsorbing aerosols that we chose is very small ( $m_i \sim 10^{-7}$ ) and do not affect our retrieval of black carbon. The refractive index of the 2nd inclusion does not affect our retrieval because the fraction of black carbon has already been determined when the 2nd inclusion is added (Section 4.1).

The retrieved black carbon fractions deduced with the nonwater hosts are 13-17 percent lower relative to black carbon fractions for water hosts; 13 percent for sea salt, 15 percent for ammonium sulfate, 15 percent for dust, and 17 percent for ammonium nitrate. The discrepancy increases as the host real refractive index increases ( $m_r = 1.49$  for sea salt, 1.53 for ammonium sulfate, 1.56 for dust and ammonium nitrate at the  $0.55 \mu\text{m}$  wavelength). Black carbon concentration is directly proportional to black carbon fraction and the black carbon specific absorption is inversely proportional to black carbon fraction (Equations 6 and 7). Hence, the corresponding black carbon concentrations inferred from nonwater hosts are 13-17 percent lower and the specific absorptions are 13-17 percent higher than for water hosts.

Some additional comments are required for dust. Dust is often considered an absorbing aerosol, but the amount of absorption is unknown. Recent studies indicate that a single value for the dust refractive index is not accurate for all locations, and that atmospheric dust is less absorbing than previously advocated (IPCC, 2001). For instance, recent *in situ* observations showed a dust refractive index of  $m = 1.53 - 0.0006i$  and a specific absorption of only  $0.009 \text{ m}^2 \text{ g}^{-1}$  for Asian aerosols advected over the Pacific Ocean (Clarke et al., 2004). We used imaginary refractive indices of 0.0024, 0.0007, 0.001, and 0.002 at the AERONET scanning wavelengths (0.44, 0.67, 0.87, and  $1.02 \mu\text{m}$ ) for our dust sensitivity test, based upon the AERONET climatologies at Bahrain-Persian Gulf, Saudi Arabia Solar Village, and Cape Verde dust sites (Dubovik et al., 2002). Locations dominated by dust hosts that are more absorbing than our dust optical model may produce errors greater than the 15 percent quoted above (especially for low fractions of black carbon), but not necessarily. For instance, a monochromatic

dust imaginary refractive index of  $m_i = 0.008i$  only increases the error to about 16 percent for this test. Given the current uncertainty for the refractive index of dust, we attempt to avoid applying our retrieval in dusty regions at present.

It is interesting to note that the small range of differences in refractive indices between the nonwater hosts results in only a 4 percent discrepancy amongst that subset, much smaller than their discrepancy with the water host ( $m_r = 1.33$  at  $0.55 \mu\text{m}$  for water). We chose water as the host for our retrieval because it is ubiquitous in the atmosphere and expected to be a component of hygroscopic tropospheric aerosols, but the choice of another host aerosol may be more appropriate in dry regions. The potentially high bias in black carbon fraction associated with inappropriate use of a water host is offset somewhat by the Maxwell Garnett effective medium approximation that produces lower absorptions than position averaging (Fuller et al., 1999). The sensitivity of our retrieval to the real refractive index of the host aerosol is further illustrated in Section 5.2.

### 5.2. Parameterization of Imaginary Refractive Index for Internal Aerosol Mixtures

Although the Maxwell Garnett effective medium approximation is accurate for inclusion size parameters as large as 0.5 (Chylek et al., 2000), many authors still use a volume averaged refractive index for aerosol mixtures. The volume averaged refractive index of an aerosol mixture is calculated by weighting the refractive index of the component aerosols with their corresponding volume fractions in the mixture. While the simplicity of this approach is attractive for computer algorithms, optical constants are not additive in general (Bohren and Huffman, 1983; p.444). We offer a simple alternative here.

The refractive index is an intrinsic property; therefore, it is independent of the particle size distribution. We use Equations (2)-(4) to plot the imaginary refractive index of three mixtures of nonabsorbing aerosols and black carbon in Figure 7. Here, the symbols represent the Maxwell Garnett calculations and the line represents the results of volume averaged calculations. Two of the mixtures consist of nonabsorbing host aerosols with black carbon inclusions, while the third mixture consists of a black carbon host with nonabsorbing inclusions. Note that the volume averaged imaginary refractive index is independent of the real refractive index, so a single line suffices for all three mixtures. The real refractive index  $m_r = 1.33$  was chosen to represent water at the  $0.55 \mu\text{m}$  wavelength; likewise,  $m_r = 1.5$  was chosen to approximate other common atmospheric aerosols such as ammonium sulfate ( $m_r = 1.53$ ), ammonium nitrate ( $m_r = 1.56$ ), and sea salt ( $m_r = 1.49$ ). In humid environments a real refractive index between 1.33 and about 1.5 can be expected for the host aerosol composite. A black carbon refractive index of  $m = 2 - 1i$  was used for all three mixtures.

The imaginary refractive index is a smooth function of the black carbon volume fraction for the Maxwell Garnett calculations of all three mixtures (symbols in Figure 7). We limit the figure to black carbon fractions of less than 0.2, but the smooth relationship for the Maxwell Garnett calculations is exhibited for all black carbon fractions. A 2nd-order polynomial is required to accurately describe the imaginary refractive index at all black carbon fractions for the two mixtures with nonabsorbing hosts:

$$m_i(\lambda) = C_0(m_r, \lambda) + C_1(m_r, \lambda)f_{bc} + C_2(m_r, \lambda)f_{bc}^2, \quad (8)$$

where  $f_{bc}$  is the volume fraction of black carbon. The coefficients  $C_i$  are dependent upon the real refractive index and

the wavelength. The imaginary refractive index of the mixture with a black carbon host can be described with a linear relationship (i.e.,  $C_2 = 0$  in Equation 8). The coefficients  $C_i$  are given for the  $0.55 \mu\text{m}$  wavelength and several refractive indices in Table 3.

Calculations for aerosol mixtures with a black carbon host and nonabsorbing inclusions are often called “inverted Maxwell Garnett” mixtures because these aerosols are not observed in the atmosphere, but we have included them in Figure 7 for completeness. Our results indicate that these elusive aerosols are closely approximated by volume averaging. If we take the other two Maxwell Garnett calculations as the “truth,” then volume averaging produces imaginary refractive index errors of 13–30 percent at black carbon fractions of 0.2. Similarly, using volume-averaged refractive indices to infer the black carbon fraction from the imaginary refractive index would produce errors of 13–23 percent for the same mixture. There is a maximum 13-percent variation in the Maxwell Garnett imaginary refractive index calculations for the two refractive indices shown in Figure 7, which is the minimal volume-averaged error. Typical aerosol hosts such as hydrated sea salt and ammonium sulfate will have a real refractive index between 1.33 and 1.5 and a composite refractive index in the shaded area of Figure 7. Hence, Table 3 can be used with any estimate of the real refractive index between 1.33 and 1.5 to produce  $m_i$  values somewhere in the shaded region, which is a better estimate of  $m_i$  than obtained from volume averaging.

We can also use Figure 7 to expand the sensitivity study of Section 5.1. In that section, we used real AERONET data with our retrieval to assess the range of black carbon fractions obtained when assuming different host aerosols. Similarly, one could use Figure 7 to infer a black carbon fraction associated with an AERONET imaginary refractive index (for the mixture) and a host real refractive index. For instance, a retrieved imaginary refractive index of 0.05 implies a black carbon volume fraction of 0.059 for a host refractive index of 1.5. The same retrieved refractive index (0.05) implies a black carbon volume fraction of 0.068 for a host refractive index of 1.33. This represents a discrepancy of about 15 percent, or midrange of the values found in Section 5.1.

### 5.3. Refractive Index and Density of Particulate Carbon

There is considerable uncertainty in the refractive index of atmospheric soot (Horvath, 1993; Chylek et al., 1995; Fuller et al., 1999; Bergstrom et al., 2002). The absorbing component of atmospheric soot is graphitic carbon (Rosen et al., 1978; 1982) which has a refractive index of  $m = 2.67 - 1.34i$  at a wavelength of  $0.54 \mu\text{m}$  (Borghesi and Guizzetti, 1991) and a density of  $2.26 \text{ g cm}^{-3}$  (Hess and Herd, 1993). Vitreous carbon, on the other hand, has a refractive index of  $m = 1.75 - 0.75i$  and a density of  $1.5 \text{ g cm}^{-3}$  (Janzen, 1979). Refractive indices in the atmospheric literature span this range and beyond (Marley et al., 2001).

Early measurements on carbon blacks by Sempflebent and Benedict (1918) indicated a refractive index of  $m = 1.95 - 0.66i$  between  $0.45$  and  $0.65 \mu\text{m}$ , according to Twitty and Weinman (1971) and Janzen (1979). Twitty and Weinman (1971) compiled a list of refractive index measurements on soots that were available at the time and chose  $m = 1.80 - 0.5i$  as representative of the  $0.25$  to  $15 \mu\text{m}$  wavelength range. This value has been widely adopted by the atmospheric research community. Indeed, the value of  $m = 1.75 - 0.44i$  at the  $0.55 \mu\text{m}$  wavelength given in the Optical Properties of Aerosols and Clouds (OPAC) databases is based upon the Twitty and Weinman survey (d’Almeida et al., 1991; Hess et al., 1998). Janzen (1979) argues that

these earlier measurements are not applicable at particulate scales because of optical inhomogeneities and used Mie theory to measure the refractive index of  $0.375\text{-}\mu\text{m}$  radii carbon blacks suspended in solution. By assuming a constant refractive index throughout the  $0.3 - 1 \mu\text{m}$  wavelength range they inferred a value of  $m = 2 - 1i$ . These various refractive index measurements were labeled Soot A ( $m = 1.95 - 0.66i$ ), Soot B ( $m = 1.80 - 0.5i$ ), and Soot G ( $m = 2 - 1i$ ) by Fuller et al. (1999); we use the same nomenclature here.

The range of specific absorption that can be calculated for the retrievals at the GSFC site (year 2000) using three black carbon refractive indices (Soot G, graphite, and OPAC) is shown in Figure 4. We tested but do not show results for Soot A and Soot B because they fall within the range of results shown; Soot A produces results very close to graphite, Soot B produces results slightly greater than OPAC soot. There is a factor of 2 variation in the results, with the highest specific absorption obtained for Soot G. Note that the value of specific absorption calculated using the OPAC soot increases by a factor of 2 if we use the soot density of  $1 \text{ g cm}^{-3}$  that is often utilized in transport models; however, we have been unable to find documented measurements of a soot density so low. We use the optical properties of the commercial carbon black Soot G in all of our calculations and outline the reasons in the following paragraphs.

The optical and physical properties of commercial carbon blacks are often used as a surrogate for atmospheric soot because they are manufactured using the same physical process (incomplete combustion). Individual carbon blacks are composed of spherical arrangements of concentric graphite platelets with decreasing graphitization near the center (Hess and Herd, 1993), which is a similar morphology to diesel soot (Clague et al., 1999; Wentzel et al., 2003). The carbon content of the two particulates differ significantly, however; diesel soot are approximately 47 percent carbon while carbon blacks are typically 95–98 percent carbon (Clague et al., 1999), indicating a high degree of impurity in the diesel soot.

The impurities affect both the refractive index and the density of the particulates, but this will not drastically alter our retrievals if the impurities are not too absorbing. We consider the nonabsorbing impurities to be either part of the host or part of the 2nd aerosol inclusion in the model that we outlined in Section 4.1. These impurities can be considered as part of the 2nd inclusion in our model if the fraction of impurities is small enough. Since our retrieval of black carbon is dependent only upon the host aerosol refractive index (and not the 2nd inclusion), small fractions of impurities will not affect our black carbon retrieval. However, if the concentration of impurities is large enough the impurities will effectively become the host aerosol. In this case, we can expect black carbon retrieval errors similar to those outlined in Section 5.1 (if we erroneously assumed a water host), or 13–17 percent for impurities with real refractive indices of 1.49–1.56.

Absorbing aerosols such as dust and organic carbon will induce errors in the retrieved values for black carbon. We have avoided using our black carbon retrieval in regions dominated by dust, but organic carbon is produced by the same incomplete combustion processes as black carbon (Seinfeld and Pandis, 1998). Organic aerosols have spectrally dependent absorption coefficients in general, typically with peak values at ultraviolet wavelengths (Jacobson, 1999). Ultraviolet wavelength absorption will not affect our visible wavelength radiometric retrieval, but the absorption tail may reach visible wavelengths for some organic carbon species. (Organic carbon aerosols with significant absorption at the AERONET retrieval wavelengths of  $0.44$ ,  $0.67$ ,  $0.87$ , and  $1.02 \mu\text{m}$  will contaminate the black carbon retrieval.) Complicating matters further, hundreds of aerosol species form the mixtures of organic carbon found in urban and remote regions, each with its own spectral absorption

signature (Seinfeld and Pandis, 1998). Sato et al. (2003) used a specific absorption of  $0.95 \text{ m}^2 \text{ g}^{-1}$  and an imaginary refractive index of 0.013 ( $\lambda = 0.5 \mu\text{m}$ ) as generic values for all organic carbon species in their study (based upon unpublished measurements). This imaginary refractive index is quite small compared with all accepted values for soot (about 0.44 to 1). Measured organic carbon concentrations vary significantly within about a factor of 7 of black carbon concentrations (Seinfeld and Pandis, 1998; Allen et al., 1999), so we conservatively estimate a positive bias of less than about 9 percent in our retrieval of black carbon when organic carbon aerosols are present (we obtain the 9 percent estimate by using volume averaging:  $7 \times 0.013/1.0 = 9$ , but note that estimates based upon volume averaging produce a high bias, as shown in Figure 7). Small hollow carbon spheres can be described using the Maxwell Garnett effective medium approximation (Bohren, 1986), and if this result holds true for complex porous soot then our model requires that we use the optical and physical properties of the dense material surrounding the pores. We chose the optical properties of the carbon black Soot G instead of pure graphite because it represents nearly pure carbon (97 percent), has a similar morphology to atmospheric aerosols, and produces yearly-averaged specific absorption close to the commonly accepted value of  $10 \text{ m}^2 \text{ g}^{-1}$  (Huffman, 1996) inferred from in situ measurements (see Table 1).

For consistency with the optical properties above we use the density of carbon blacks in our retrieval. We chose a density of  $2 \text{ g cm}^{-3}$  because that is a midrange value of available pycnometer and X-ray diffraction measurements. The lowest pycnometer measurements on carbon blacks indicate densities of  $1.85 \text{ g cm}^{-3}$  and the highest X-ray diffraction measurements indicate densities of  $2.11 \text{ g cm}^{-3}$  (Hess and Herd, 1993). Black carbon concentration and specific absorption are directly and inversely proportional to the black carbon density (see Eqs. 6 and 7) so these extremes represent deviations of 7.5 and 5.5 percent.

## 6. Comments on Mixture Assumptions

There is considerable evidence that a significant fraction of black carbon is internally mixed with sulfate and water, which we review here. Both soot and sulfate are produced by incomplete combustion processes which renders their concentrations highly correlated and provides an opportunity for internal mixing (Pinnick et al., 1993; Krivacsy et al., 2001). Indeed, analysis of electron microscope photographs over Europe during LACE98 indicate that more than 50 percent of the soot is internally mixed with sulfate aerosols (Ebert et al., 2002). Transport models require wet deposition of black carbon in order to obtain reasonable residence times in the atmosphere, indicating that this hydrophobic aerosol is somehow drawn into the hydrological cycle. Sulfate aerosols are highly hygroscopic and provide a mechanism for the embedment of soot into fine mode particulate matter (i.e., radii less than about  $0.6 \mu\text{m}$ ) and the hydrological cycle that is consistent with observations and models. Finally, specific absorptions of  $10 \text{ m}^2 \text{ g}^{-1}$  or more that are commonly observed in the atmosphere can not be achieved with external mixtures of observed aerosol size distributions (Fuller et al., 1999).

At this time, the refractive index retrievals in the AERONET database provide a single value for all aerosol particle sizes. Hence, we chose to model a mixture of aerosols that approximates the AERONET method for our black carbon retrieval, or equal fractions of black carbon in the fine and coarse modes with an effective refractive index for the mixture. However, fine and coarse mode aerosols are created by different mechanisms and can not be expected to

share the same fraction of black carbon. We discuss possible repercussions of using a uniform mixture of aerosols for all particle sizes in Section 6.1.

Additionally, the Maxwell Garnett effective medium approximation that we use in our retrieval is rigorously valid only when the inclusions in the aerosol mixture are small with respect to the radiative wavelength. Numerous studies have shown, however, that this assumption may be relaxed to include inclusion size parameters ( $2\pi r/\lambda$ ) of at least 0.5. We discuss the morphology of atmospheric soot in Section 6.2 and the sensitivity of absorption to the size of the inclusions in Section 6.3.

### 6.1. Inclusion of Black Carbon in the Coarse Mode

Soot particles near sources are small and unimodal with radii of about  $0.05 \mu\text{m}$  (Steiner et al., 1992; Venkataraman and Friedlander, 1994; Berner et al., 1996; Kleeman et al., 2000; Bond et al., 2002). Like all submicron aerosols, however, soot is not expected to aggregate into the coarse mode; coarse mode aerosols are created by other processes such as mechanical generation by surface winds. Nonetheless, up to 25 percent of the elemental carbon mass is contained in the coarse mode of urban and biomass burning aerosols (Maenhaut et al., 1996; Virkkula et al., 1999; Neusub et al., 2002b). Modal mass fractions of elemental carbon vary from 10-22 percent for the fine mode particulate and 2-12 percent for the coarse mode. This indicates that the small carbon particles are attached to larger particles, as also seen in Clark et al. (2004).

We have included equal fractions of black carbon in the fine and coarse modes because it is inherently assumed in the AERONET retrievals that all particles have the same refractive index (Dubovik and King, 2000). The AERONET retrievals are constrained to match measured radiances and can be expected to accurately describe the radiance field; including black carbon in the fine mode without including it the coarse mode would alter the optical properties and nullify the radiative constraints that are the foundation of the original retrieval. Sensitivity studies indicate that the AERONET retrieval provides refractive indices between the actual fine and coarse mode values when retrieving bimodal aerosol distributions (Dubovik et al., 2000), indicating that artificial absorption deduced in one mode is somewhat offset by decreased absorption deduced in the other mode. The specific absorptions and black carbon concentrations discussed here are constrained by the refractive index and size distributions inferred from the AERONET retrievals (see Section 4.1), which in turn constrains the absorption optical depth. We emphasize that although we are required to include black carbon in the coarse mode in order to constrain the retrieval to the AERONET refractive index, this does not imply that *large* black carbon particles are included in the coarse mode. On the contrary, the black carbon inclusions are always assumed to be small whenever one implements the Maxwell Garnett effective medium approximation. Soot particle size is discussed further in the next two subsections.

We estimate the error associated with assuming equal fractions of black carbon in the fine and coarse modes through a sensitivity study. Dubovik et al. (2000) tested the AERONET retrieval on a bimodal aerosol size distribution that was dominated by fine mode aerosols having a very different complex refractive index than the coarse mode aerosols; they used  $r_{v,f} = 0.118$ ,  $r_{v,c} = 1.17$ ,  $\sigma_f = \sigma_v = 0.6$ , and  $C_{v,f}/C_{v,c} = 2$  in Equation (1), a fine mode refractive index of  $m = 1.65 - 0.035i$ , and a coarse mode refractive index  $m = 1.33 - 0.0005i$ . The fine mode imaginary refractive index of this test distribution can be achieved with a volume mixture of 3.8 percent black carbon in a nonabsorbing host with a refractive index of  $m = 1.63 - 0i$ ; the coarse

mode refractive index is consistent with a slightly absorbing aerosol containing less than 0.1 volume percent of black carbon. Taking both modes together, this test size distribution has a black carbon volume concentration of 2.5 percent [ $3.8 \times C_{v,f} / (C_{v,f} + C_{v,c})$ ]. The refractive index returned by the AERONET retrieval is  $m = 1.52 - 0.023i$ , from which we retrieve a black carbon volume fraction of 3.2 percent by assuming a water host aerosol and using the techniques of Section 4.1. This is a relative error in black carbon concentration of 28 percent [ $(3.2/2.5 - 1) \times 100$ ].

Obviously, this sensitivity study is not representative of the abundance of possible black carbon mixing scenarios, and larger errors are possible. However, large errors in the black carbon concentration will produce unreasonable values for the specific absorption (see Eq. 7). Although reasonable yearly-averaged specific absorptions with small standard deviations are retrieved at all locations (see Table 1), the accuracies of individual black carbon retrievals have not been measured. Coincident elemental carbon measurements throughout the atmospheric column are required to validate the inferred black carbon concentrations. The most reliable results are expected to occur when the black carbon volume fraction is the same in both the fine and coarse modes, or when the aerosol size distribution is nearly monomodal.

## 6.2. Soot Aggregates

Atmospheric soot is often observed as aggregates of primary black carbon spheres (or monomers) in transmission electron microscopy images (Martins et al., 1998; Ebert et al., 2002; Li et al., 2003a, 2003b; Wentzel et al., 2003). Aggregate clusters with linear branches of monomers are said to be “open,” whereas nonbranched clumps of monomers are said to be “closed.” Both open and closed soot clusters have been observed in the atmosphere. Primary particle radii for diesel soot aggregates are about 0.003–0.011  $\mu\text{m}$ , corresponding to size parameters of 0.05–0.14 at a wavelength of 0.5  $\mu\text{m}$  (Wentzel et al., 2003). However, motor vehicle emission measurements typically show radii of 0.05  $\mu\text{m}$  (size parameter of 0.63 at a wavelength of 0.5  $\mu\text{m}$ ), indicating some aggregation at the source (Steiner et al., 1992; Venkataraman and Friedlander, 1994; Kleeman et al., 2000). The small primary particles that aggregate into clusters are often surrounded by highly hygroscopic ammonium sulfate (Ebert et al., 2002), and aging in conditions of high relative humidity breaks the aggregate chains into smaller clusters again (Hallet et al., 1989).

The aggregate soot can be adequately modeled with Mie theory if the primary particles are not too large. Mulholland et al. (1994) used the coupled electric and magnetic dipole method to show that open aggregates of 17, 52, and 165 spheres with monomer size parameters of less than 0.5 have the same specific absorption as a loose collection of single spheres to within 10 percent. Fuller (1995) obtained a maximum 14 percent difference for similar calculations using 5-carbon aggregates (closed-packed and linear chains) with monomer size parameters less than 0.57.

## 6.3. Soot Monomer Size

Rigorous application of the Maxwell Garnett mixing rule requires a uniform electric field throughout the inclusions, or equivalently, monomer size parameters much less than 1 (Bohren, 1986; Chylek et al., 2000). However, testing of specific cases by some authors has shown that this restriction may be relaxed for monomer size parameters as large as 0.5. We highlight several of these cases in the following paragraphs.

One method of testing an effective medium approximation is by comparison to “position averaging.” With position averaging, the absorption of a single eccentric inclusion is averaged over all possible positions within a nonabsorbing

host aerosol. The single-position calculations can be done very accurately, and position averaging is often the basis for comparisons to effective medium approximations. Fuller et al. (1999) used position averaging and a multiple-reflection model to calculate the specific absorption of black carbon inclusions in a sulfate host (0.55  $\mu\text{m}$  wavelength). They assumed a polydisperse size distribution for this internal mixture with a mass median radius of 0.21  $\mu\text{m}$  and a geometric standard deviation of 2.0. They varied the mass fraction of black carbon from 0.01 to 0.2. They found the Maxwell Garnett specific absorption calculations to be 6 percent less than the position-averaged calculations.

Another method for testing effective medium approximations is the discrete dipole method, which provides an exact solution for multiple absorbing inclusions in a host aerosol. Chylek et al. (2000) used this method to model multiple carbon inclusions in water droplets as a basis for comparison to the Maxwell Garnett effective medium approximation. The black carbon volume fraction was held constant at 10 percent in their study, but the size parameter of the inclusions was varied from 0.33 to 1.44. They found the extinction and scattering efficiencies of the two methods to differ by less than 4 percent for inclusion size parameters below 0.55. Absorption efficiencies differed by about twice that much, or 8 percent.

Martins et al. (1998) also used the discrete dipole approximation to assess the efficacy of Maxwell Garnett theory. They modeled closed soot clusters with nonabsorbing coatings; the mixture size parameters ranged from 0.57 to 4.7. The soot cluster was maintained at 52 percent of the volume of the mixture, and monomer soot size parameters of 0.65 were used in the largest mixtures. We emphasize that the size of their soot cluster was seven times larger than the monomers and essentially the same size as the mixture. Nonetheless, the specific absorptions that they calculated (0.55  $\mu\text{m}$  wavelength) using the Maxwell Garnett effective medium approximation were within 10 percent of the exact values. This is particularly significant because of the large soot fraction used for this test.

We also used the concentric sphere tests of Dubovik et al. (2000) to estimate the error associated with locating all black carbon in a sphere at the center of the particles (rather than many small particles mixed throughout). The two tests utilize the bimodal biomass burning size distributions of their Table 2 ( $r_{v,f} = 0.132$ ,  $r_{v,c} = 4.5$ ,  $\sigma_f = 0.4$ ,  $\sigma_c = 0.6$ ,  $C_{v,f}/C_{v,c} = 4$ ) with either fixed radius carbon cores of 0.038  $\mu\text{m}$  or carbon cores with fixed radius ratios of  $r_{core}/r_{shell} = 0.33$  at all sizes in the distribution. These two scenarios represent a black carbon volume fraction of 0.043 for the fixed radius core and a black carbon volume fraction of 0.036 for the fixed ratio case. The AERONET retrieval infers a refractive index of  $m = 1.46 - 0.02i$  for the fixed radius core and a refractive index of  $m = 1.44 - 0.02i$  for the fixed ratio case. Using a black carbon refractive index identical to the one used by Dubovik et al. (2000) for consistency ( $m_{bc} = 1.65 - 0.45i$ ), we retrieved a black carbon volume fraction of 0.049 for both test cases. This is 14 percent more black carbon than the concentric sphere model with a fixed radius core, and 36 percent more black carbon than the concentric sphere model with a fixed radius ratio. Note that extremely large black carbon particles are included in the fixed ratio test case (particle sizes up to 4.95  $\mu\text{m}$  radius, or size parameters up to 56.5 at a wavelength of 0.55  $\mu\text{m}$ ) which violates the small particle assumption of the Maxwell Garnett effective medium approximation.

The bias of the errors summarized in this section may be negative or positive, depending upon the volumes of the particles and the sizes and fractions of the soot inclusions (Videen et al., 1994; Martins et al., 1998; Fuller et al., 1999; Chylek et al., 2000). Generally, theoretical studies indicate that the Maxwell Garnett effective medium approximation underestimates the absorption (i.e., a negative bias)

for small particles and small fractions of black carbon, but the bias changes sign for large particles. Hence, we conclude that the Maxwell Garnett mixing rule is accurate to approximately  $\pm 10$  percent for aerosol mixtures with randomly located black carbon inclusions, as long as the size parameters of the monomers are no greater than 0.5–0.6.

## 7. Conclusions

Continuous worldwide measurements of black carbon concentrations are required to improve the current gridded carbon emissions inventories and transport models. Black carbon specific absorption measurements are also desirable for relating the modeled microphysics to aerosol optical properties. We have developed a technique for retrieving both the black carbon column concentration and specific absorption from the worldwide AERONET database.

Particulate carbon absorbs visible radiation more efficiently when it is contained within a host aerosol (i.e., internal versus external mixing) but the increase in efficiency is not uniform for all internal mixtures of aerosols. We calculated the range of possible specific absorptions for internal mixtures of black carbon using nine climatological size distributions, and found a factor of 2 or more variability for black carbon fractions typical of atmospheric aerosols. The results are highly dependent upon the volume fraction of black carbon but independent of specific combustion processes, as we used a single refractive index for black carbon in this study. This indicates that a single number can not be used to accurately convert thermal black carbon concentration measurements to absorption (and vice versa) without knowledge of the aerosol size distribution and fraction of black carbon.

We used the Maxwell Garnett effective medium approximation to infer the column-averaged concentration and specific absorption of black carbon associated with the AERONET retrievals at 46 locations. The yearly-averaged black carbon column concentrations that we found are comparable to typical measured concentrations if a 1 km boundary layer is assumed:  $0.22\text{--}0.28 \mu\text{g m}^{-3}$  at remote island locations,  $0.96\text{--}3.47 \mu\text{g m}^{-3}$  in continental regions, and  $2.7\text{--}3.7 \mu\text{g m}^{-3}$  in biomass burning locations (see Table 2). Likewise, the specific absorptions we infer at these locations are consistent with other reported values. The ocean sites have a higher specific absorption (averaging  $11.3 \text{ m}^2 \text{ g}^{-1}$  for 2200 retrievals) and the biomass burning sites have a lower specific absorption ( $8.9 \text{ m}^2 \text{ g}^{-1}$  for 3942 retrievals) than the continental sites ( $9.9 \text{ m}^2 \text{ g}^{-1}$  for 13,449 retrievals) because of the inverse relationship of specific absorption to black carbon concentration.

We also used the Maxwell Garnett effective medium approximation to parameterize the imaginary refractive index with respect to the black carbon volume fraction, enabling simple but accurate absorption estimates for aerosol mixtures when the black carbon fraction is known. The parameterization indicates that the mixture imaginary refractive index is sensitive to the real refractive index of the host aerosol, but not to additional inclusions. We compared our parameterization to the volume-averaged mixing approximation and found a 13–30 percent high bias for volume-averaged imaginary refractive index and the host aerosols tested; this corresponds to a 13–23 percent low bias in the inferred black carbon concentration if volume averaging is substituted for the Maxwell Garnett equations in our retrieval. The high bias for the imaginary refractive index produced by the volume mixing approximation is very similar to an “inverted Maxwell Garnett” mixture consisting of a black carbon host aerosol with nonabsorbing inclusions.

Our approach probably represents an upper limit to the black carbon concentration and a lower limit to the specific absorption (if all of the black carbon is internally mixed with

equal fractions in the fine and coarse modes). We assumed a water aerosol host, and this will result in black carbon concentrations that are 13–17 percent too high in regions where other common aerosols are a more appropriate host. The presence of organic carbon will induce a retrieved black carbon bias of about 10 percent or less for organic to elemental carbon mass ratios of 7 or less. Absorbing dust will also produce a similar bias in our black carbon retrieval. The Maxwell Garnett effective medium approximation and uncertainty in the density of black carbon adds uncertainties of  $\pm 15$  and  $\pm 5$  percent to the retrieved black carbon. A simple sum of all these uncertainties indicates a possible bias of  $-15$  to  $+40$  percent in our black carbon concentration retrieval. Our results are effectively constrained by the absorption optical depth in the AERONET database, so the corresponding uncertainty in the black carbon specific absorption is  $+15$  to  $-40$  percent (e.g., Equation 7). The black carbon concentrations derived here represent an improvement over the factor of 2+ uncertainty in the black carbon emissions inventories. The specific absorptions represent an improvement over using a single value for a parameter that varies by a factor of 4.

Uncertainty in published values of the black carbon refractive index could potentially alter our results by a factor of 2, but we require the retrieval to produce reasonable values for the black carbon specific absorption. We used a refractive index corresponding to a highly graphitized carbon, or  $m = 2 - 1i$ , which results in an average specific absorption of  $10 \text{ m}^2 \text{ g}^{-1}$  for 19,391 retrievals; this is the commonly accepted value.

The retrieval technique presented here enables a comparison between model estimates of black carbon concentrations and worldwide AERONET measurements. We emphasize that this is an optical retrieval based upon surface radiance measurements, and as such we can only provide “optically equivalent” results; we have not validated our results with elemental carbon measurements throughout the atmospheric column. Nonetheless, the black carbon concentrations and specific absorptions that we deduce from AERONET measurements correctly describe the surface radiance field.

**Acknowledgments.** This work was funded by the Earth Science Enterprise and the Clouds and Earth’s Radiant Energy System (CERES) project. We appreciate the efforts of the AERONET team and the instrument principle investigators: Norm O’Neill, John Vande Castle, Mary Jane Bartholomew, Paulo Artaxo, Didier Tanre, Giuseppe Zibordi, Michel Verbrughe, Gian Paolo Gobbi, Arnon Karnieli, Madar Egert, Ramesh Singh, Ken Voss, Bruce McArthur, Doug Moore, Phillippe Goloub, Stuart Piketh, Joo-Wan Cha, Vinod Tare, Sachchida Nand Tripathi, Robert Frouin. We thank Wenying Su, Bill Grant, Tom Charlock, and two anonymous reviewers for careful reading of the paper that resulted in significant improvements.

## References

- Ackerman, A.S., O.B. Toon, D.E. Stevens, A.J. Heymsfield, V. Ramanathan, E.J. Welton, Reduction of tropical cloudiness by soot, *Science*, 288, 1042–1047, 2000.
- Ackerman, T.P., O.B. Toon, Absorption of visible radiation in atmosphere containing mixtures of absorbing and nonabsorbing particles, *Appl. Opt.*, 20 (20), 3661–3668, 1981.
- Allen, G.A., J. Lawrence, P. Koutrakis, Field validation of a semi-continuous method for aerosol black carbon (aethalometer) and temporal patterns of summertime hourly black carbon measurements in southwestern PA, *Atmos. Environ.*, 33, 817–823, 1999.
- Arnott, W.P., H. Moosmuller, P.J. Sheridan, J.A. Ogren, R. Raspet, W.V. Slaton, J.L. Hand, S.M. Kreidenweis, J.L. Collet, Photoacoustic and filter-based ambient aerosol light absorption measurements: Instrument comparisons and the role of relative humidity, *J. Geophys. Res.*, 108(D1), 4034, doi: 10.1029/2002JD002165, 2003.

- Bansal, R.C., J. Donnet, Mechanism of black carbon formation, in *Carbon Black*, J. Donnet, R. Bansal, M. Wang, eds., 67-88, Marcel Dekker, New York, 1993.
- Bergstrom, R.W., P.B. Russell, P. Hignett, Wavelength dependence of the absorption of black carbon particles: predictions and results from the TARFOX experiment and implications for the aerosol single scattering albedo, *J. Atmos. Sci.*, 59, 567-577, 2002.
- Berner, A., S. Sidla, Z. Galambos, C. Kruisz, R. Hitzenberger, H.M. ten Brink, G.P.A. Kos, Modal character of black carbon size distributions, *J. Geophys. Res.*, 101 (D14), 19559-19565, 1996.
- Bohren, C.F., Applicability of effective-medium theories to problems of scattering and absorption by nonhomogeneous atmospheric particles, *J. Atmos. Sci.*, 43 (5), 468-475, 1986.
- Bohren, C.F., D.R. Huffman, *Absorption and scattering of light by small particles*, Wiley, New York, 1983.
- Bond, T.C., R.J. Charlson, J. Heintzenberg, Quantifying the emission of light-absorbing particles: Measurements tailored to climate studies, *Geophys. Res. Lett.*, 25 (3), 337-340, 1998.
- Bond, T.C., D.S. Covert, J.C. Kramlich, T.V. Larson, R.J. Charlson, Primary particle emissions from residential coal burning: Optical properties and size distributions, *J. Geophys. Res.*, 107 (D21), 8347, doi: 10.1029/2001JD000571, 2002.
- Borghesi, A., G. Guizzetti, Graphite (C), in *Handbook of Optical Constants of Solids II*, E.D. Palik, ed., 449-460, Academic Press, 1991.
- Bruce, C.W., T.F. Stromberg, K.P. Gurton, J.B. Mozer, Trans-spectral absorption and scattering of electromagnetic radiation by diesel soot, *Applied Optics*, 30(12), 1537-1546, 1991.
- Charlock, T.P., W.D. Sellers, Aerosol effects on climate: Calculations with time-dependent and steady-state radiative-convective models, *J. Atmos. Sci.*, 37, 1327-1341, 1980.
- Charlson, R.J., J. Langner, H. Rodhe, H. Rodhe, C.B. Leovy, S.G. Warren, Perturbation of the northern hemisphere radiative balance by backscattering from anthropogenic sulfate aerosols, *Tellus*, 43A, 152-163, 1991.
- Charlson, R.J., S.E. Schwartz, J.M. Hales, R.D. Cess, J.A. Coakley, J.E. Hansen, D.J. Hofman, Climate forcing by anthropogenic aerosols, *Science*, 255, 423-430, 1992.
- Chylek, P., J.A. Coakley, Aerosols and Climate, *Science*, 183, 75-77, 1974.
- Chylek, P., G. Videen, D. Ngo, R. Pinnick, J. Klett, Effect of black carbon on the optical properties and climate forcing of sulfate aerosols, *J. Geophys. Res.*, 100 (18), 16325-16332, 1995.
- Chylek, P., G. Videen, et al., Effective medium approximations for homogeneous particles, in *Light Scattering by Nonspherical Particles: Theory, Measurements, and Geophysical Applications*, M. Mishchenko, ed., p273-308, Academic, San Diego, CA, 2000.
- Clague, A.D.H., J.B. Donnet, T.K. Wang, J.C.M. Peng, A comparison of diesel engine soot with carbon black, *Carbon*, 37, 1553-1565, 1999.
- Clarke, A.D., et al., Size distributions and mixtures of dust and black carbon aerosol in Asian outflow: Physiochemistry and optical properties, *J. Geophys. Res.*, 109, D15S09, doi:10.1029/2003JD004378, 2004.
- Colbeck, I., B. Atkinson, Y. Johar, The morphology and optical properties of soot produced by different fuels, *J. Aerosol Sci.*, 28(5), 715-723, 1997.
- Collins, W.D., P.J. Rasch, et al., Simulating aerosols using a chemical transport model with assimilation of satellite aerosol retrievals: Methodology for INDOEX, *J. Geophys. Res.*, 106 (D7), 7313-7336, 2001.
- Cooke, W.F., C. Lioussé, H. Cahier, J. Feichter, Construction of a 1x1 degree fossil fuel emission data set for carbonaceous aerosol and implementation and radiative impact in the ECHAM4 model, *J. Geophys. Res.*, 104 (D18), 22137-22162, 1999.
- d'Almeida, G.A., P. Koepke, E.P. Shettle, *Atmospheric Aerosols: Global Climatology and Radiative Characteristics*, A. Deepak, Hampton, Virginia, 1991.
- Delene, D.J., J. Ogren, Variability of aerosol optical properties at four North American surface monitoring sites, *J. Atmos. Sci.*, 59, 1135-1150, 2002.
- Dubovik, O., M.D. King, A flexible inversion algorithm for retrieval of aerosol optical properties from sun and sky radiance measurements, *J. Geophys. Res.*, 105 (D16), 20673-20696, 2000.
- Dubovik, O., A. Smirnov, B. Holben, M.D. King, Y.J. Kaufman, T.F. Eck, I. Slutsker, Accuracy assessments of aerosol optical properties retrieved from Aerosol Robotic Network (AERONET) sun and sky radiance measurements, *J. Geophys. Res.*, 105 (D8), 9791-9806, 2000.
- Dubovik, O., B. Holben, T. Eck, A. Smirnov, Y. Kaufman M. King, D. Tanre, I. Slutsker, Variability of absorption and optical properties of key aerosol types observed in worldwide locations, *J. Atmos. Sci.*, 59, 590-608, 2002.
- Ebert, M., S. Weinbruch, A. Rausch, G. Gorzawski, P. Hoffmann, H. Wex, G. Helas, Complex refractive index of aerosols during LACE 98 as derived from the analysis of individual particles, *J. Geophys. Res.*, 107 (D21), 8121, doi:10.1029/2000JD000195, 2002.
- Fuller, K.A., Scattering and absorption cross sections of compounded spheres: II. Calculations for external aggregation, *J. Opt. Soc. Am. A.*, 12(5), 881-892, 1995.
- Fuller, K.A., W.C. Malm, S.M. Kreidenweis, Effects of mixing on extinction by carbonaceous particles, *J. Geophys. Res.*, 104 (D13), 15941-15954, 1999.
- Hallet, J., J.G. Hudson, C.F. Rogers, Characterization of combustion aerosols for haze and cloud formation, *Aerosol Sci. Tech.*, 10, 70-83, 1989.
- Hansen, J., L. Nazarenko, Soot climate forcing via snow and ice albedos, *PNAS*, 101 (2), 423-428, 2004.
- Harshvardhan, Aerosol-Climate interactions, in *Aerosol-Cloud-Climate Interactions*, P.J. Hobbs, ed., 75-95, Academic Press, New York, 1993.
- Hartley, W.S., P.V. Hobbs, J.L. Ross, P.B. Russell, J.M. Livingston, Properties of aerosols aloft relevant to direct radiative forcing of the mid-Atlantic coast of the United States, *J. Geophys. Res.*, 105(D8), 9859-9885, 2000.
- Haywood, J.M., K.P. Shine, The effect of anthropogenic sulfate and soot on the clear sky planetary radiation budget, *Geophys. Res. Lett.*, 22 (5), 603-606, 1995.
- Haywood, J.M., K.P. Shine, Multi-spectral calculations of the direct radiative forcing of tropospheric sulphate and soot aerosols using a column model, *Q.J.R. Meteorol. Soc.*, 123, 1907-1930, 1997.
- Hegg, D.A., J. Livingston, P.V. Hobbs, T. Novakov, P. Russell, Chemical apportionment of aerosol column optical depth off the mid-Atlantic coast of the United States, *J. Geophys. Res.*, 102 (D21), 25293-25303, 1997.
- Hess, W.H., C.R. Herd, Microstructure, morphology, and general physical properties, in *Carbon Black*, J. Donnet, R. Bansal, M. Wang, eds., 89-173, Marcel Dekker, 1993.
- Hess, M., P. Koepke, I. Schult, Optical properties of aerosols and clouds: the software package OPAC, *Bull. Am. Meteor. Soc.*, 79 (5), 831-844, 1998.
- Holben, B.N., et al, AERONET - A federated instrument network and data archive for aerosol characterization, *Remote Sens. Environ.*, 66, 1-16, 1998.
- Holben, B.N., et al., An emerging ground-based aerosol climatology: Aerosol optical depth from AERONET, *J. Geophys. Res.*, 106 (D11), 12067-12097, 2001.
- Horvath, H., Atmospheric light absorption - a review, *Atmos. Environ.*, 27A(3), 293-317, 1993.
- Huffman, H.D., Comparison of the light absorption coefficient and carbon measures for remote aerosols: an independent analysis of data from the IMPROVE network - I, *Atmos. Environ.*, 30(1), 73-83, 1996.
- IPCC, 2001: Climate Change 2001: The Scientific Basis. Contribution of Working Group I to the Third Assessment Report of the Intergovernmental Panel on Climate Change [Houghton, J.T., Y. Ding, D.J. Griggs, M. Noguer, P.J. van der Linden, X. Dai, K. Maskell, and C.A. Johnson (eds.)]. Cambridge University Press, Cambridge, United Kingdom and New York, NY, USA, 881pp.
- Jacobson, M.Z., Development and application of a new air pollution modeling system - Part III. Aerosol-phase simulations, *Atmos. Environ.*, 31(4), 587-608, 1997.
- Jacobson, M.Z., Isolating nitrated and aromatic aerosols and nitrated aromatic gases as sources of ultraviolet light absorption, *J. Geophys. Res.*, 104(D3), 3527-3542, 1999.
- Jacobson, M.Z., Strong radiative heating due to the mixing state of black carbon in atmospheric aerosols, *Nature*, 409, 695-697, 2001.

- Janzen, J., The refractive index of colloidal carbon, *J. Colloid and Interface Science*, 69(3), 436-447, 1979.
- Kinne, S., et al., Monthly averages of aerosol properties: A global comparison among models, satellite data, and AERONET ground data, *J. Geophys. Res.*, 108 (D20), doi:10.1029/2001JD001253, 2003.
- Kleeman, M.J., J.J. Schauer, G.R. Cass, Size and composition distribution of fine particulate matter emitted from motor vehicles, *Environ. Sci. Tech.*, 34(7), 1132-1142, 2000.
- Krivacsy, Z., A. Hoffer, Z. Sarvari, D. Temesi, U. Baltensperger, S. Nyeki, E. Weingartner, S. Kleefeld, S.G. Jennings, Role of organic and black carbon in the chemical composition of atmospheric aerosol at European background sites, *Atmos. Environ.*, 35, 6231-6244, 2001.
- Lesins, G., P. Chylek, U. Lohmann, A study of internal and external mixing scenarios and its effects on aerosol optical properties and direct radiative forcing, *J. Geophys. Res.*, 107 (D10), 10.1029/2001JD000973, 2002.
- Li, J., J. R. Anderson, P.R. Buseck, TEM study of aerosol particles from clean and polluted marine boundary layers over the North Atlantic, *J. Geophys. Res.*, 108 (D6), 4189, doi:10.1029/2002JD002106, 2003a.
- Li, J., M. Posfai, P.V. Hobbs, P.R. Buseck, Individual aerosol particles from biomass burning in southern Africa: 2. Compositions and aging of inorganic particles, *J. Geophys. Res.*, 108 (D13), 8484, doi:10.1029/2002JD002310, 2003b.
- Liou, S.C., H. Cachier, S.G. Jennings, Optical and thermal measurements of black carbon aerosol content in different environments: variation of the specific attenuation cross-section, sigma, *Atmos. Environ.*, 27A (8), 1203-1211, 1993.
- Liou, S.C., J.E. Penner, C. Chuang, J.J. Walton, H. Eddleman, H. Cachier, A global three-dimensional model study of carbonaceous aerosols, *J. Geophys. Res.*, 101 (D14), 19411-19432, 1996.
- Maenhaut, W., I. Salma, J. Cafmeyer, H.J. Annegarn, M.O. Andreae, Regional atmospheric aerosol composition and sources in the eastern Transvaal, South Africa, and impact of biomass burning, *J. Geophys. Res.*, 101 (D19), 23631-23650, 1996.
- Malm, W.C., J.F. Sisler, D. Huffman, R.A. Eldred, T.A. Cahill, Spatial and seasonal trends in particle concentration and optical extinction in the United States, *J. Geophys. Res.*, 99(D1), 1347-1370, 1994.
- Marley, N.A., J.S. Gaffney, J.C. Baird, et al., An empirical method for the determination of the complex refractive index of size-fractionated atmospheric aerosols for radiative transfer calculations, *Aer. Sci. Tech.*, 34, 535-549, 2001.
- Martins, J.V., P. Artaxo, C. Liou, J.S. Reid, P.V. Hobbs, Y.J. Kaufman, Effects of black carbon content, particle size, and mixing on light absorption by aerosols from biomass burning in Brazil, *J. Geophys. Res.*, 103 (D4), 32041-32050, 1998.
- Moosmuller, H., W.P. Arnott, C.F. Rogers, J.C. Chow, C.A. Frazier, L.E. Sherman, D.L. Dietrich, Photoacoustic and filter measurements related to aerosol light absorption during the Northern Front Range Air Quality Study (Colorado 1996/1997), *J. Geophys. Res.*, 103 (D1), 28149-28157, 1998.
- Mulholland, G.W., C.F. Bohren, K.A. Fuller, Light scattering by agglomerates: Coupled electric and magnetic dipole method, *Langmuir*, 10, 2533-2546, 1994.
- Myhre, G., F. Stordal, K. Restad, I.S.A. Isaksen, Estimation of the direct radiative forcing due to sulfate and soot aerosols, *Tellus*, 50B, 463-477, 1998.
- Neusub, C., T. Gnauk, A. Plewka, H. Herrmann, and P. K. Quinn, Carbonaceous aerosol over the Indian Ocean: OC/EC fractions and selected specifications from size-segregated onboard samples, *J. Geophys. Res.*, 107(D19), 8031, doi:10.1029/2001JD000327, 2002a.
- Neusub, C., H. Wex, W. Birmili, A. Wiedensohler, C. Koziar, B. Busch, E. Brüggemann, T. Gnauk, M. Ebert, D.S. Covert, Characterization and parameterization of atmospheric particle number-, mass-, and chemical-size distributions in central Europe during LACE 98 and MINT, *J. Geophys. Res.*, 107(D21), 8127, doi:10.1029/2001JD000514, 2002b.
- Novakov, T., Soot in the atmosphere, in *Particulate Carbon*, G. Wolff and R. Klimisch eds., 19-41, Plenum Press, New York, 1982.
- Park, R.J., D.J. Jacob, M. Chin, R.V. Martin, Sources of carbonaceous aerosols over the United States and implications for natural visibility, *J. Geophys. Res.*, 108(D12), 4355, doi:10.1029/2002JD003190, 2003.
- Penner, J.E., C.C. Chuang, K. Grant, Climate forcing by carbonaceous and sulfate aerosols, *Climate Dynamics*, 14, 839-851, 1998.
- Penner, J.E., R.E. Dickinson, C.A. O'Neill, Effects of aerosol from biomass burning on the global radiation budget, *Science*, 256, 1432-1434, 1992.
- Petzold, A., C. Kopp, R. Niessner, The dependence of the specific attenuation cross-section on black carbon mass fraction and particle size, *Atmos. Environ.*, 31(5), 661-672, 1997.
- Pinnick, R.G., G. Fernandez, E. Martinez-Andazola, B.D. Hinds, A.D.A. Hansen, K. Fuller, Aerosol in the arid Southwestern United States: Measurements of mass loading, volatility, size distribution, absorption characteristics, black carbon content, and vertical structure to 7 km above sea level, *J. Geophys. Res.*, 98(D2), 2651-2666, 1993.
- Rosen, H., A.D.A. Hansen, L. Gundel, T. Novakov, Identification of the optically absorbing component in urban aerosols, *Applied Optics*, 17 (24), 3859-3861, 1978.
- Rosen, H., A.D.A. Hansen, R.L. Dod, L.A. Gundel, T. Novakov, Graphitic carbon in urban environments and the Arctic, in *Particulate Carbon*, G. Wolff and R. Klimisch eds., 273-294, Plenum Press, New York, 1982.
- Sato, M., J. Hansen, D. Koch, A. Lacis, R. Ruedy, O. Dubovik, B. Holben, M. Chin, T. Novakov, Global atmospheric black carbon inferred from AERONET, *Proc. Nat. Acad. Sci.*, 100, (11), 6319-6324, 2003.
- Schult, I., J. Feichter, W.F. Cooke, Effect of black carbon and sulfate aerosols on the global radiation budget, *J. Geophys. Res.*, 102 (D25), 30107-30117, 1997.
- Schwartz, S.E., The whitehouse effect - shortwave radiative forcing of climate by anthropogenic aerosols: an overview, *J. Aerosol Sci.*, 27 (3), 359-382, 1996.
- Seinfeld, J.H., S.N. Pandis, *Atmospheric Chemistry and Physics*, Wiley, New York, 1998.
- Steiner, D., H. Burtscher, H. Gross, Structure and disposition of particles from a spark-ignition engine, *Atmos. Environ.*, 26A (6), 997-1003, 1992.
- Streets, D.G., S. Gupta, S.T. Waldhoff, M.Q. Wang, T.C. Bond, B. Yiyun, Black carbon emissions in China, *Atmos. Environ.*, 35, 4281-4296, 2001.
- Toon, O.B., T.P. Ackerman, Algorithms for the calculation of scattering by stratified spheres, *Applied Optics*, 20(20), 3657-3660, 1981.
- Toon, O.B., J.B. Pollack, B.N. Khare, The optical constants of several atmospheric aerosol species: Ammonium Sulfate, Aluminum Oxide, and Sodium Chloride, *J. Geophys. Res.*, 81 (33), 5733-5748, 1976.
- Twitty, J.T., J.A. Weinman, Radiative properties of carbonaceous aerosols, *J. Appl. Meteorol.*, 10, 725-731, 1971.
- Venkataraman, C., S. Friedlander, Size distributions of polycyclic aromatic hydrocarbons and elemental carbon. 2. Ambient measurements and effects of atmospheric processes, *Environ. Sci. Technol.*, 28, 563-572, 1994.
- Virkkula, A., M. Aurela, R. Hillamo, T. Makela, T. Pakkanen, V. Kerminen, W. Maenhaut, F. Francois, J. Cafmeyer, Chemical composition of atmospheric aerosol in the European subarctic: Contribution of the Kola Peninsula smelter areas, central Europe, and the Arctic Ocean, *J. Geophys. Res.*, 104 (D19), 23681-23696, 1999.
- Wentzel, M., H. Gorzawski, K.-H. Naumann, H. Saathoff, S. Weinbruch, Transmission electron microscopical and aerosol dynamical characterization of soot aerosols, *Aerosol Science*, 34, 1347-1370, 2003.
- Wiscombe, W.J., Improved Mie scattering algorithms, *Appl. Opt.*, 19(9), 1505-1509, 1980.

Gregory L. Schuster NASA Langley Research Center Mail Stop 420 Hampton, VA 23681 USA. (gregory.l.schuster@nasa.gov)

Oleg Dubovik Laboratory for Terrestrial Physics, Code 923 NASA Goddard Space Flight Center Greenbelt, Maryland 20771 USA. Also at Goddard Earth Science and Technology Center University of Maryland Baltimore County 1000 Hilltop Circle Baltimore, Maryland 21250 USA.

Brent N. Holben Laboratory for Terrestrial Physics, Code 923 NASA Goddard Spaceflight Center Greenbelt, Maryland, 20771 USA.

Eugene E. Clothiaux Department of Meteorology 503 Walker Building The Pennsylvania State University University Park, Pennsylvania, 16802 USA.

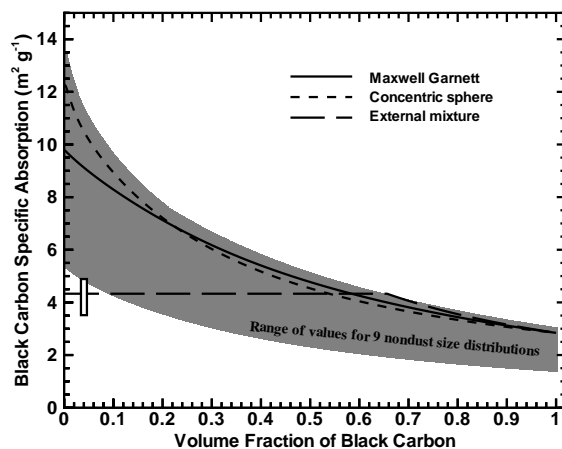


**Figure 1.** Black carbon specific absorption ( $\lambda = 0.55 \mu\text{m}$ ) inferred from size distribution climatologies in Dubovik et al. (2002) and black carbon mixed with ammonium sulfate. The shaded area indicates the range of results for internal mixtures of all nine nondust size distributions. Lines represent calculations using the GSFC distribution, including the Maxwell Garnett (solid line), concentric sphere (dashed line), and external mixture morphologies (long dashes). The bar indicates the range of specific absorption calculated for all nine distributions with external mixtures of black carbon in the fine mode.

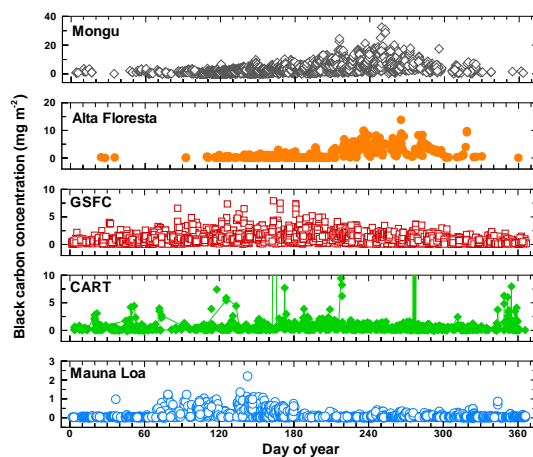


**Figure 2.** Black carbon concentration calculated using the AERONET retrievals at 5 locations from 1993 through 2002 (note the difference in scales). Seasonal variations at the biomass burning sites (Mongu and Alta Floresta) and the urban site (GSFC) are obvious.

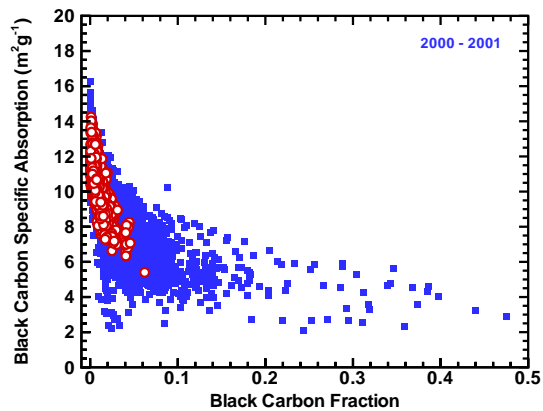


**Figure 3.** Black carbon specific absorption at the 0.55  $\mu\text{m}$  wavelength and black carbon fraction calculated at 46 AERONET sites for all successful retrievals in the years 2000 and 2001. The GSFC site is highlighted with circles. A refractive index of  $m = 2 - 1i$  and a density of  $2 \text{ g cm}^{-3}$  was used for black carbon.

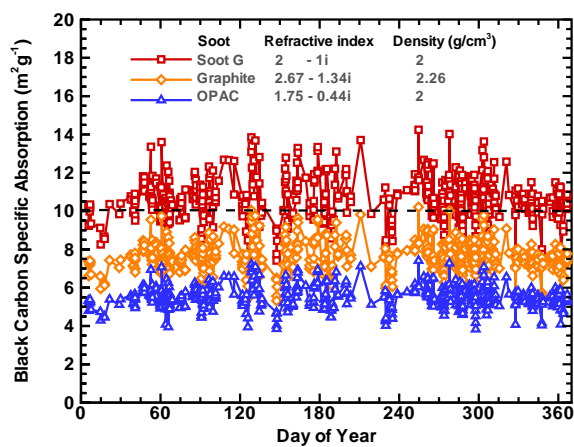


**Figure 4.** Daily variability of specific absorption in the year 2000 at the GSFC AERONET site. Results are shown for 3 different soots, but only Soot G produces values near  $10 \text{ m}^2 \text{ g}^{-1}$ .

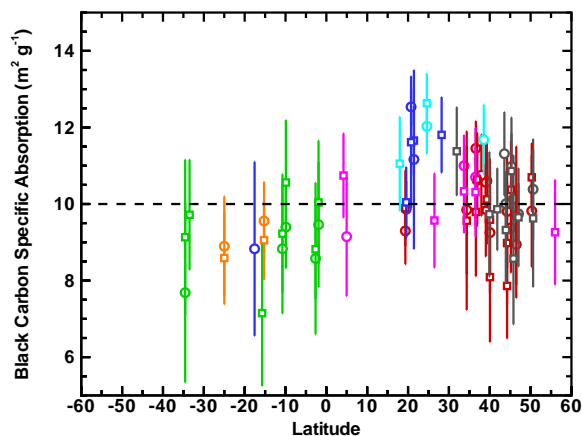


**Figure 5.** Yearly averaged specific absorption at the AERONET sites in Table 1. Circles represent the year 2000, squares the year 2001; whiskers indicate the standard deviations. Colors represent various regions, including North America (red), Europe (grey), Asia (purple), South America (green), Africa (orange), Atlantic Islands (light blue), Pacific Islands (dark blue).

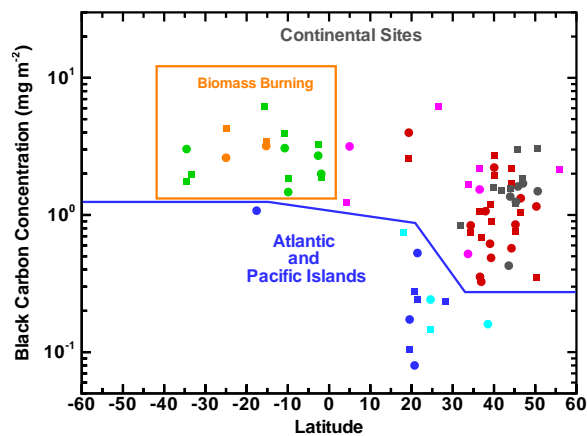


**Figure 6.** Black carbon concentration corresponding to the AERONET sites in Table 1. Circles represent the year 2000, squares the year 2001. Colors represent various regions, including North America (red), Europe (grey), Asia (purple), South America (green), Africa (orange), Atlantic Islands (light blue), Pacific Islands (dark blue).

**Table 1.** Yearly averaged specific absorption ( $\alpha$ ;  $\text{m}^2 \text{g}^{-1}$ ), standard deviations, and number of retrievals at 46 AERONET sites for the years 2000 and 2001.

| SITE                                  | Lat     | 2000     |      |      | 2001     |      |      |
|---------------------------------------|---------|----------|------|------|----------|------|------|
|                                       |         | $\alpha$ | s.d. | pts. | $\alpha$ | s.d. | pts. |
| <b>North &amp; Central America</b>    |         |          |      |      |          |      |      |
| Bratts Lake                           | 50.280  | 9.8      | 1.5  | 108  | 10.7     | 0.9  | 135  |
| Rimrock                               | 46.487  | 8.9      | 1.4  | 235  | 9.7      | 1.8  | 260  |
| Howland                               | 45.200  | 9.4      | 1.2  | 100  | 10.4     | 1.3  | 285  |
| HJAndrews                             | 44.239  | 9.8      | 1.5  | 265  | 7.9      | 1.4  | 306  |
| Egbert                                | 44.226  | .        | .    |      | 9.0      | 1.6  | 202  |
| BONDVILLE                             | 40.053  | 9.3      | 1.6  | 183  | 9.6      | 1.6  | 295  |
| BSRN BAO Boulder                      | 40.045  | .        | .    |      | 8.1      | 1.7  | 430  |
| MD Science Center                     | 39.283  | 10.6     | 1.0  | 548  | 10.1     | 1.2  | 813  |
| GSFC                                  | 39.030  | 10.6     | 1.1  | 565  | 9.8      | 1.2  | 607  |
| Wallops                               | 37.942  | 10.8     | 1.1  | 150  | .        | .    |      |
| COVE                                  | 36.900  | 10.6     | 1.2  | 183  | 10.6     | 1.2  | 575  |
| CART                                  | 36.600  | 11.5     | 0.7  | 279  | 9.8      | 1.7  | 281  |
| Sevilleta                             | 34.355  | 9.8      | 1.7  | 552  | 9.6      | 2.3  | 575  |
| Mexico City                           | 19.334  | 9.3      | 0.9  | 184  | 9.9      | 1.0  | 79   |
| <b>South America</b>                  |         |          |      |      |          |      |      |
| Balbina                               | -1.917  | 9.5      | 1.6  | 72   | 10.0     | 1.6  | 100  |
| Belterra                              | -2.648  | 8.6      | 2.0  | 76   | 8.8      | 1.3  | 110  |
| Alta Floresta                         | -9.917  | 9.4      | 1.1  | 113  | 10.6     | 1.6  | 142  |
| Abracos Hill                          | -10.760 | 8.8      | 1.7  | 140  | 9.2      | 1.5  | 128  |
| CUIABA MIRANDA                        | -15.729 | .        | .    |      | 7.2      | 1.9  | 308  |
| Santiago                              | -33.490 | .        | .    |      | 9.7      | 1.4  | 89   |
| CEILAP BA                             | -34.567 | 7.7      | 2.3  | 349  | 9.1      | 2.0  | 315  |
| <b>Europe &amp; Mediterranean Sea</b> |         |          |      |      |          |      |      |
| Lille                                 | 50.612  | 10.4     | 1.3  | 96   | 9.6      | 1.8  | 95   |
| Moldova                               | 47.033  | 9.7      | 0.8  | 237  | 9.7      | 1.3  | 315  |
| Ispra                                 | 45.803  | 10.1     | 1.1  | 297  | 8.6      | 1.7  | 459  |
| Venise                                | 45.314  | 11.0     | 1.3  | 437  | 10.9     | 1.0  | 140  |
| Avignon                               | 43.933  | 10.0     | 0.8  | 305  | 9.3      | 1.4  | 234  |
| Toulouse                              | 43.575  | 11.3     | 1.1  | 90   | .        | .    |      |
| Rome Tor Vergata                      | 41.840  | .        | .    |      | 9.9      | 1.1  | 401  |
| IMC Oristano                          | 39.910  | .        | .    |      | 9.7      | 1.6  | 210  |
| Nes Ziona                             | 31.922  | .        | .    |      | 11.4     | 1.2  | 152  |
| <b>South Africa</b>                   |         |          |      |      |          |      |      |
| Mongu                                 | -15.254 | 9.6      | 1.0  | 532  | 9.1      | 1.0  | 778  |
| Skukuza                               | -24.992 | 8.9      | 1.3  | 312  | 8.6      | 1.2  | 378  |

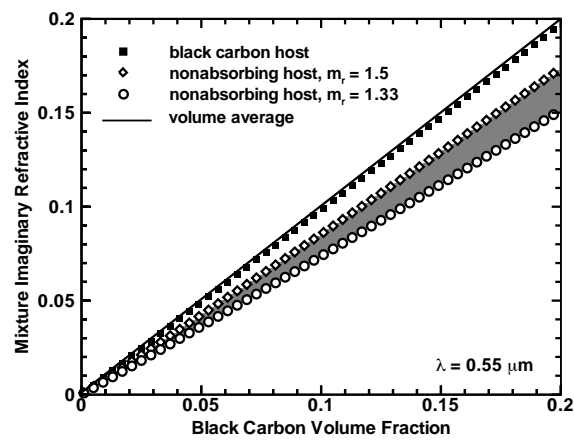


**Figure 7.** Imaginary refractive index of composite aerosols calculated using the Maxwell Garnett equations for various mixtures of black carbon and nonabsorbing aerosols. Circles are calculated for a host real refractive index of 1.33 with black carbon inclusions, diamonds are similarly calculated for a host real refractive index of 1.5, and squares are calculated for a black carbon host with inclusions having a real refractive index of 1.5. The line is calculated using volume averaging and very closely approximates the case with a black carbon host. A black carbon refractive index of  $m = 2 - 1i$  was used in all cases.

**Table 2.** Yearly regional averages of black carbon concentration ( $[BC]$ ;  $\text{mg m}^{-2}$ ), specific absorption ( $\alpha$ ;  $\text{m}^2 \text{g}^{-1}$ ), and number of retrievals for the years 2000 and 2001.

| SITE                   | 2000  |          |      | 2001  |          |      |
|------------------------|-------|----------|------|-------|----------|------|
|                        | [BC]  | $\alpha$ | pts. | [BC]  | $\alpha$ | pts. |
| <b>Continental</b>     |       |          |      |       |          |      |
| North & Central Amer   | 0.957 | 10.2     | 3352 | 1.218 | 9.7      | 4843 |
| Europe                 | 1.384 | 10.4     | 1462 | 1.914 | 9.6      | 2006 |
| Asia                   | 1.648 | 10.5     | 395  | 3.468 | 10.0     | 1391 |
| <b>Biomass Burning</b> |       |          |      |       |          |      |
| South America          | 2.668 | 8.4      | 750  | 3.299 | 8.9      | 1192 |
| South Africa           | 2.972 | 9.3      | 844  | 3.693 | 8.9      | 1156 |
| <b>Remote</b>          |       |          |      |       |          |      |
| Atlantic Islands       | 0.263 | 11.9     | 364  | 0.283 | 12.3     | 406  |
| Pacific Islands        | 0.227 | 10.4     | 727  | 0.217 | 11.2     | 703  |

**Table 3.** Empirical parameters for approximating the Maxwell Garnett imaginary refractive index of a mixture of inclusions in a host aerosol using Equation (8). Wavelength =  $0.55 \mu\text{m}$ .

| Host $m_r$ | Inclusion $m_r$ | $C_0$   | $C_1$  | $C_2$  |
|------------|-----------------|---------|--------|--------|
| 1.33       | 2.0             | 0.0043  | 0.6600 | 0.3348 |
| 1.35       | 2.0             | 0.0036  | 0.6838 | 0.3122 |
| 1.4        | 2.0             | 0.0021  | 0.7398 | 0.2590 |
| 1.45       | 2.0             | 0.0008  | 0.7906 | 0.2103 |
| 1.5        | 2.0             | -0.0002 | 0.8366 | 0.1659 |
| 1.55       | 2.0             | -0.0010 | 0.8780 | 0.1257 |
| 1.6        | 2.0             | -0.0017 | 0.9152 | 0.0894 |
| 2.0        | 1.5             | -0.0027 | 0.9970 |        |
| volume avg | 2.0             | 0.0     | 1.0    |        |